UNIVERSIDADE DE BRASÍLIA – INSTITUTO DE GEOCIÊNCIAS

CURSO DE PÓS-GRADUAÇÃO EM GEOCIÊNCIAS APLICADAS

TESE DE DOUTORADO N° 09

Análise de incertezas e inversão conjunta para aprimoramento da modelagem crustal

Área de concentração: Geofísica Aplicada

LUCAS PAES MOREIRA

Orientador: Prof. Dr. George Sand Leão Araújo de França (Universidade de Brasília)

Co-orientador: PhD Michael James Friedel (*United States Geological Survey*)

Brasília DF

2013

Universidade de Brasília
Instituto de Geociências

Análise de incertezas e inversão conjunta para aprimoramento da modelagem crustal

Autor*
Lucas Paes Moreira

Orientador:
Prof. Dr. George Sand Leão Araújo de França (Univ. de Brasília – Brasil)

Co-orientador:
PhD Michael James Friedel (*United States Geological Survey* – Estados Unidos)

Tese apresentada ao Instituto de Geociências da Universidade de Brasília, para a obtenção do título de Doutor em Geociências Aplicadas, na área de Geofísica Aplicada.

Brasília DF
2013

* Este trabalho contou com apoio financeiro do CAPES.

Lucas Paes Moreira

Análise de incertezas e inversão conjunta para aprimoramento da modelagem crustal

Tese apresentada ao Instituto de Geociências da Universidade de Brasília, para a obtenção do título de Doutor em Geociências Aplicadas, na área de Geofísica Aplicada.

Autor: Lucas Paes Moreira

Orientador: Prof. Dr. George Sand Leão Araújo de França (Univ. de Brasília)

Co-orientador: PhD Michael James Friedel (*United States Geological Survey*)

Brasília DF
2013

Moreira, Lucas Paes.
Análise de incertezas e inversão conjunta para aprimoramento da modelagem crustal
80 páginas
Tese de Doutorado – Instituto de Geociências da Universidade de Brasília.

1. Inversão conjunta
2. Análise de incertezas
3. Função do receptor
4. Dispersão de ondas superficiais
5. Magnetotelúrico

I. Universidade de Brasília. Instituto de Geociências.

Comissão Julgadora:

Prof. Dr. George Sand Leão Araújo de França

Prof. Dr. Mônica Giannoccaro von Huelsen

Prof. Dr. Marcelo Peres Rocha

Prof. Dr. Marcelo Sousa de Assumpção

Prof. Dr. João Carlos Dourado

Agradecimentos

Gostaria de agradecer a todos que contribuiram direta e indiretamente para a realização dessa tese de doutorado. Em especial minha família, pelo apoio incondicional, incentivo e paciência nas horas mais difíceis.

Registro também um agradecimento ao professor orientador e amigo George Sand França, que incentivou e convenceu a iniciar essa etapa, que culminou na conclusão desse trabalho. Agradeço também ao professor Reinhardt Fuck, pela confiança e disponibilização da bolsa de estudos, essencial para o desenvolvimento da pesquisa. Um agradecimento especial ao co-orientador e amigo Michael Friedel, que me acolheu durante minha estada nos exterior e contribuiu integralmente para e pesquisa realizada. Agradeço também os membros da banca de avaliação por disponibilizarem seu tempo para ler e avaliar esse trabalho, dando contribuições significativas para sua conclusão.

Finalmente um agradecimento aos companheiros Cristiano Chimpliganond, Sidinei Tomás e Umberto Travaglia que motivaram, acompanharam e contribuiram para o desenvolvimento do trabalho.

Esse trabalho contou com o financiamento de bolsa de estudos do CAPES através do Instituto Nacional de Ciência e Tecnologia para Estudos Tectônicos e de bolsa de doutorado sanduíche CAPES/Fulbright 23038.034805/2009-71.

Abstract

Moreira, L.P. **Uncertainty analysis and joint inversion for improvement of crustal imaging**. XX pp, doctoral dissertation. University of Brasília, Brazil, 2013.

The aim of this work is to present two new methodologies to improve crustal imaging using joint inversion of multiple data set. The first proposed method is the uncertainties analysis of the joint inversion of receiver function and surface waves dispersion. Joint inversions of these two data groups have recently become popular due to the improvement to reduce the non-uniqueness of seismic velocities imaging. However, the uncertainties of calibrated models are usually overlooked or ignored and the methodologies applied for uncertainty assessment have no formal formulation. It is proposed a quantitative method for uncertainty assessment using observation samples prediction, usually applied for hydro-geophysics and environment modeling. The methodology is tested in synthetic data and applied in field data collected from the seismic station POPB, part of the Brazilian Lithospheric Seismic Project, located in the Paraná Basin, southeast Brazil. The results of these tests show reliable range of values for the inverted parameters from 0.111–0.412 km/s (2.5% – 9.2%), and 0.110–0.341 km/s (2.5% – 7.9%) for synthetic and field tests respectively. The second proposed method is the joint inversion of receiver function, surface waves dispersion and magnetotelluric data for 2D crust modelling. The inversion methodology uses a Gauss-Marquardt-Levenberg algorithm to minimize a multi-component objective function with a cross-gradient constraint (geometric structure similarity of different physical parameters). The proposed procedure was tested using synthetic data from realistic 1D seismic models co-located with a 2D magnetotelluric profile. Results show improved resolution in the estimated resistivity structure compared to the traditional inversion of resistivity parameters using only magnetotelluric data. Improvements include resolving lateral variations and depth of discontinuities, and a high-resistivity zone underlying a high-conductivity zone (500-fold contrast). For the seismic 1D models, the absolute values of layer shear-wave velocity are closer (+/-3%) to the synthetic model crustal structures demonstrating benefits of the joint inversion.

Resumo

Moreira, LP **Análise de incerteza e inversão conjunta para aprimoramento da modelagem crustal**. XX pp, tese de doutorado. Universidade de Brasília, Brasil, 2013.

O objetivo deste trabalho é apresentar duas novas metodologias para aprimorar a modelagem crustal usando inversão conjunta de múltiplos dados geofísicos. O primeiro método proposto é a análise das incertezas da inversão conjunta da função do receptor e dispersão de ondas superficiais. Inversões conjuntas destes dois grupos de dados estão se tornando populares devido à capacidade de reduzir a não-unicidade em modelos de velocidades de ondas sísmicas. No entanto, as incertezas dos modelos calibrados são geralmente negligenciadas ou ignoradas e as metodologias utilizadas não possuem formulação formal. É proposto, portanto, um método quantitativo de determinação de incertezas a partir da predição de amostras observadas, normalmente aplicada para hidro-geofísica e modelagem ambiental. A metodologia é testada em dados sintéticos e aplicada em dados de campo coletados pela estação sismográfica POPB, parte do Brazilian Lithospheric Seismic Project, localizada na Bacia do Paraná, sudeste do Brasil. Os resultados obtidos nesses testes mostram uma faixa de valores dos parâmetros invertidos de 0,111 a 0,412 km/s (2,5% a 9,2%), e 0,110 a 0,341 km/s (2,5% a 7,9%) para os testes com dados sintéticos e de campo, respectivamente. O segundo método proposto é a inversão conjunta de função do receptor, dispersão de ondas de superfície e dados magnetotelúricos para modelagem crustal 2D. A metodologia de inversão usa o algoritmo de Gauss-Marquardt-Levenberg para minimizar uma função objectivo multi-componente com um vínculo estrutural do gradiente cruzado (similaridade estrutural geométrica dos diferentes parâmetros físicos). O procedimento proposto foi testado utilizando dados sintéticos de modelos realísticos de perifs 1D de velocidade de ondas sísmicas co-localizados com um perfil 2D de resistividade. Os resultados mostram uma melhora na estrutura de resistividade estimada em comparação com a inversão de parâmetros de resistividade utilizando apenas dados magnetotelúricos. As melhorias incluem a resolução de variações laterais da profundidade das descontinuidades, e a identificação da zona de alta resistividade subjacente a uma zona de alta condutividade. Para os modelos 1D de velocidades de ondas sísmicas, os valores absolutos da velocidade de onda S das camadas do perfil são próximos dos valores sintéticos (+ / - 3%), demonstrando os benefícios da inversão conjunta.

Sumário

Agradecimentos i
Abstract ii
Resumo iii
Sumário iv
Lista de figuras v
Lista de tabelas vii
Abreviaturas e siglas viii

1. Introdução 1
    1.1. Apresentação da tese 4
    1.2. Referências 4

2. Uncertainty Analysis in the Joint Inversion of Receiver Function and Surface-Wave Dispersion, Paraná Basin, Southeast Brazil 7
    2.1. Introduction 8
    2.2. Methodology 9
        2.2.1. Linearized inversion 9
        2.2.2. Prediction 12
    2.3. Synthetic test 16
        2.3.1. Receiver functions 17
        2.3.2. Surface wave dispersion 18
        2.3.3. Joint inversion 19
        2.3.4. Observation prediction and uncertainty analysis 22
    2.4. Application to field data 27
    2.5. Conclusions 31
    2.6. Data and resources 32
    2.7. Acknowledgements 33
    2.8. References 33

3. Joint inversion of receiver function, surface wave dispersion, and magnetotelluric data for 2D crustal modeling 39
    3.1. Introduction 40
    3.2. Methodology 42
        3.2.1. Forward model 42
            3.2.1.1. Receiver function 42
            3.2.1.2. Surface wave dispersion 43
            3.2.1.3. Magnetotelluric 45
        3.2.2. Joint inversion 46
        3.2.3. Cross-gradient constraint 47
    3.3. Synthetic test 49
        3.3.1. Separate inversions 51
        3.3.2. Joint inverion 57
    3.4. Conclusions 60
    3.5. Computational resources 60
    3.6. Acknowledgements 61
    3.7. References 61

4. Conclusões 67

Lista de figuras

Figure 2.1 – Non-linear system with two model parameters p1 and p2. (a) Objective function surface with a minimum region (gray area) defined as sufficient to consider the model optimal. (b) Increasing direction of one particular observation sample based on parameters variation. (c) Combination of these two pictures showing the maximum and minimum critical values for the estimated model. (d) Increasing direction of other particular observation sample. (e) Maximum and minimum critical values for the second observation. (f) Four critical points representing four model parameter combinations inside the objective function estimation threshold region. (adapted with permission from Doherty, 2005) 15

Figure 2.2 – 1D profile used to generate synthetic seismograms used in the joint inversion of receiver function and surface-wave dispersion. 17

Figure 2.3 – (a) RF and SWD joint inversion results. The dashed profile represents the actual (synthetic) model, used to calculate the observation data, the solid profile represents the model estimated by the inversion, and the dotted profile is the inversion initial model. (b) RF traces of the real model (dashed) and the trace from the estimated model (solid). (c) Dispersion curves of real model (pluses) and from the estimated model (crosses). 21

Figure 2.4 – (a) RF trace and three observation samples (54, 86, 224) occurring at different time locations, (b) one-dimensional S-velocity profile obtained by maximizing (dotted lines) and minimizing (dashed lines) the 3 observation samples in (a). 23

Figure 2.5 – One-dimensional S-velocity profiles obtained from each observation sample prediction (black), profile estimated by the joint inversion (red), and model used to build the synthetic observation data (blue). 24

Figure 2.6 – Probability density functions and statistical distributions that best fit the predicted values for (a) the second layer (b) the layer just below the Conrad discontinuity, and (c) the layer just below Moho. 26

Figure 2.7 – Uncertainty in the estimated S-wave velocity profile (solid black line) including three prediction percentiles: 90th (dashed blue), 95th (dashed green), and 99th (dashed red). 27

Figure 2.8 – RF traces calculated with the time-domain deconvolution for 6 teleseismic events recorded by POPB station (dashed lines), and the stacked trace (solid line) used as observation samples in the joint-inversion process (vector **c** in equation 2.4) 29

Figure 2.9 – Global model IASP91 (dashed) used as initial values in the joint inversion process and the estimated model (solid) showing three main discontinuities: sediment-upper crust, Conrad and Moho, with depths different from the global model. 29

Figure 2.10 – (a) Predicted models for each observation sample (black) and the inversion estimated model (red). (b) Estimated model (solid black line) and the profiles corresponding to the range of percentiles: 90th (dashed blue), 95th (dashed green) and 99th (dashed red) calculated from predicted values. 31

Figure 3.1 – Discrete representation of cross-gradient constraint for a 2D grid. Adapted from Gallardo and Meju, 2004. 49

Figure 3.2 – Homogeneous synthetic model of resistivity and velocity parameters with lateral variation of layers depth and a low velocity-resistivity zone on the left portion. 50

Figure 3.3 – Calibration results for profiles N01 (top), C00 (center) and S01 (bottom), comparing the initial (dash-point), original (dashed) and estimated (solid) parameters values. 53

Figure 3.4 – Receiver function traces from original (dashed) and estimated (solid) models for the profiles N01 (top), C00 (center) and S01 (bottom) 54

Figure 3.5 – Dispersion curves from synthetic (circle) and estimated (red solid line) models for the profiles N01 (top), C00 (center) and S01 (bottom) 55

Figure 3.6 – Estimated resistivity parameters for MT inversion. The vertical resolution is limited and the true model lateral variation is not imaged. 56

Figure 3.7 – Apparent resistivity and phase for three MT stations with original (dots) and estimated (solid line) samples. 57

Figure 3.8 – Joint inversion results for N01 (top), C00 (center) and S01 (bottom) seismic profiles with synthetic (dashed) and estimated (solid) parameters values. 58

Figure 3.9 – Joint inversion results for resistivity parameters. 59

Lista de tabelas

Table 2.1 – Earthquake data used to estimate crustal velocity structure. Waveforms were obtained from the IRIS Data Management Center earthquake datacenter. 28

Abreviaturas e siglas

1D	One dimension
2D	Two dimensions
BLSP	Brazilian Lithospheric Seismic Project
IASP91	Parameterised velocity model that has been constructed to be a summary of the travel time characteristics of the main seismic phases
LVZ	Low velocity zone
Moho	Mohorovičić
MT	Magnetotelluric
RF	Receiver function
SWD	Surface wave dispersion
TE	Transverse electric
TM	Transverse magnetic

1. – Introdução

A inversão numérica representa uma importante ferramenta na determinação de modelos geofísicos realísticos e o aprimoramento dessa ferramenta tem se mostrado uma necessidade recorrente em aplicações como exploração mineral, de óleo e gás natural e modelagem de estruturas crustais. A determinação de modelos geofísicos a partir de dados observados apresenta diversas restrições e desafios, tais como instabilidade numérica, não unicidade, limitação no número de parâmetros invertidos, precisão na modelagem direta, entre outros (Tarantola, 2005).

Com a finalidade de minimizar ou eliminar tais restrições e dificuldades várias abordagens são frequentemente utilizadas para estabilização e convergência da inversão numérica. A não unicidade é causada pela ocorrência de múltiplos mínimos na função objetivo, dada pela diferença entre os valores observados e as amostras de saída do modelador direto, gerando múltiplas soluções. Esse problema pode ser contornado através da utilização de vários modelos iniciais distintos (Ammon, 1991) ou algoritmos de inversão baseados em buscas globais, tais como algoritmos evolutivos (Lawrence and Wiens 2004, An and Assumpção, 2004) ou Bayesianos (Bodin et al, 2012). A instabilidade numérica é geralmente causada pelo número excessivo de parâmetros invertidos, pela não-linearidade na relação entre parâmetros e observações e também pela ocorrência de correlação entre os diferentes parâmetros (Doherty and Johnston, 2003). Essa instabilidade pode ser minimizada através da inclusão de restrições nessas relações, como vínculos de suavidade (Tikonov e Arsenin, 1977), estruturais (Gallardo e Meju, 2007) ou inclusão de informações a priori, como por exemplo informações de parâmetros físicos conhecidos.

Diferentes dados geofísicos fornecem diferentes informações no processo de inversão, relacionando diferentes parâmetros físicos a diferentes dados observados (Gallardo e Meju, 2003, 2007; Julià et al. 2000). A relação entre esses diferentes parâmetros, portanto, pode prover informações geológicas ou estruturais não observáveis em uma análise individual. Assim, a análise conjunta da inversão numérica de diferentes dados geofísicos, fornece informação adicional na calibração e validação de modelos (Ozalaybey et al, 1997, Bedrosian et al, 2007). A inversão conjunta consiste em agregar esses diferentes dados geofísicos em um único esquema de calibração, compondo uma única função objetivo multi-componente. As informações adicionais incorporadas resultam em restrições adicionais nos dados utilizados, consequentemente

reduzindo a não-unicidade do problema, e tornando o processo mais imune a ruídos nos dados observados utilizados. O aumento no número de parâmetros invertidos, entretanto, acarreta geralmente em um aumento na instabilidade numérica no processo da inversão e por esse motivo requerem vínculos adicionais e relações matemáticas entre os diferentes parâmetros calibrados (Gallardo e Meju, 2007; Zevallos et al, 2009).

A inversão é geralmente realizada iterativamente, a partir de métodos numéricos que atualizam os valores dos parâmetros a fim de diminuir ao máximo a diferença entre os dados observados e os dados gerados por modelos computacionais (função objetivo). Por se tratar de uma solução numérica iterativa o valor mínimo da função objetivo, que hipoteticamente representa o modelo teórico que melhor se aproxima do modelo real, nem sempre é possível de ser alcançado, especialmente em problemas mal-postos (Tikonov e Arsenin, 1977), principalmente devido ao ruído nos dados observados e correlação entre os parâmetros invertidos. Isso acarreta em incertezas associadas aos modelos obtidos no processo de calibração. A determinação dessas incertezas é frequentemente negligenciada ou mesmo ignorada na calibração de modelos, e muitas vezes analisada de forma qualitativa e simplificada. No caso da inversão conjunta de dados de função do receptor e dispersão de ondas superficiais as incertezas são geralmente associadas às variâncias (ou desvio-padrão) dos parâmetros, obtidas a partir da matriz de co-variância calculada no processo de inversão, assumindo uma distribuição Normal em torno do valor estimado. Essa abordagem é falha ao assumir tal distribuição, e ignorar os demais elementos da matriz de co-variância, implicitamente sugerindo a independência entre os parâmetros invertidos, o que raramente acontece em inversão geofísica. Outros métodos mais qualitativos são usados através da calibração de modelos com diferentes subgrupos de dados observados, determinando uma faixa de valores para os parâmetros estudados. Dentre os métodos quantitativos de determinação das incertezas associadas à inversão geofísica estão os métodos Bayesianos (Gallager e Doherty, 2007) de calibração, que atualizam os parâmetros calibrados gerando distribuições a posteriori a partir de uma distribuição a priori dos parâmetros. Essa distribuição calculada representa a probabilidade de um determinado parâmetro assumir um valor específico. Esses métodos, contudo, representam as incertezas em termos probabilísticos, além de demandarem alto esforço computacional.

A presente tese tem como proposta a apresentação de metodologias que auxiliem a aprimorem a inversão de dados geofísicos. Assim, foram desenvolvidas duas metodologias a serem apresentadas: a determinação das incertezas associadas à inversão

conjunta de função do receptor e dispersão de ondas de superfície, e a inversão conjunta de dados de função do receptor, dispersão de ondas superficiais e magnetotelúrico para modelagem crustal.

A primeira metodologia propõe um método quantitativo para determinação das incertezas do processo de inversão baseado no mapeamento de uma região de confiança da função objetivo definida por um valor limiar dessa função, que representa o conjunto de diferentes modelos que podem ser considerados calibrados, ou seja, se aproximam do modelo real, gerando assim estatisticamente um intervalo de valores que cada parâmetro pode assumir dentro do intervalo de confiança. Esse mapeamento é feito através da predição de valores observados (Vecchia e Cooley, 1987). A predição consiste em determinar o maior (ou o menor) valor que uma certa observação pode assumir considerando que o modelo se mantenha calibrado, ou seja, que a função objetivo se mantenha abaixo de um limite previamente estabelecido. Esse ponto da função objetivo (valor máximo de uma observação dentro de um limiar da função objetivo), determinado por um conjunto de parâmetros define um ponto crítico. Considerando que diferentes observações são independentes entre si, e que possuem diferentes sentidos de crescimento no domínio da função objetivo, a predição de todas as amostras resultarão em pontos críticos que mapeam o contorno de uma região de mínimo da função objetivo, resultando em uma distribuição estatística de valores dos parâmetros a partir da definição de um intervalo de confiança.

A segunda metodologia propõe a inversão conjunta de três dados geofísicos distintos: traço de função do receptor, curva de dispersão de ondas superficiais e resistividade e fase de modos transverso elétrico (TE) e transverso magnético (TM) de dados magnetotelúricos. Esses dados sismológicos modelam a velocidade de ondas sísmicas em subsuperfície, que são sensíveis à densidade das rochas e suas propriedades elásticas de compressão mecânica (Aki e Richards, 1980; Berteussen, 1977), enquanto que dados magnetotelúricos modelam a resistividade das rochas (Korja, 1997; Simpson e Bahr, 2005) e são sensíveis ao conteúdo de fluidos, porosidade e conteúdo mineral (Keller, 1989). A agregação desses dois parâmetros geofísicos em um mesmo processo de inversão pode ser aprimorado levando em consideração que diferentes litologias apresentam diferentes velocidades de ondas sísmicas (Christensen and Mooney, 1995) e diferentes resistividades elétricas (Korja, 1997), e portanto descontinuidades encontradas em modelos de resisitividade elétrica presumem descontinuidades co-localizadas de velocidades de ondas sísmicas. Para realçar a presença de

descontinuidades co-localizadas em ambos modelos, um vínculo estrutural do gradiente cruzado (Gallardo e Meju, 2003, 2007) é introduzido, incorporando também um vínculo de suavidade, estabilizando a inversão numérica.

Apresentação da tese

Esta tese é dividida em quatro capítulos cuja organização é descrita a seguir:

O capítulo 1 apresenta a introdução dos assuntos a serem abordados, envolvendo as justificativas e objetivos apresentados.

No capítulo 2 é apresentado o primeiro artigo denominado "Uncertainty Analysis in the Joint Inversion of Receiver Function and Surface-Wave Dispersion, Paraná Basin, Southeast Brazil", submetido ao Bulletin of the Seismological Society of America (ISSN 0037-1106) em maio de 2012 e aceito para publicação, com data prevista para junho de 2013.

No capítulo 3 é apresentado o segundo artigo denominado "Joint inversion of receiver function, surface wave dispersion, and magnetotelluric data for 2D crustal modeling", submetido ao Journal of Applied Geophysics (ISSN 0926-9851) em fevereiro de 2013.

O capítulo 4 sintetiza as principais conclusões da pesquisa.

Referências

Aki, K. and Richards, P. G. 1980. Quantitative Seismology: Theory and Methods, Vol. 1 and 2, W. H. Freeman, San Francisco.

Ammon, C. J., 1991. The isolation of receiver effects from teleseismic P waveforms. Bull. Seismol. Soc. Amer., 81(6), 2504-2510.

An, M., and M.S. Assumpção (2004). Multi-objective inversion of surface waves and receiver functions by competent genetic algorithm applied to the crustal structure of the Parana Basin, SE Brazil, Geophys. Res. Lett. 31, L05615, doi:10.1029/2003GL019179.

Bedrosian, P.A., Maercklin, N., Weckmann, U., Bartov, Y., Ryberg, T., and Ritter, O. (2007). Lithology-derived structure classification from the joint interpretation of magnetotelluric and seismic models, Geophys. J. Int. 170, 737–748.

Berteussen, K. A. (1977). Moho depth determinations based on spectral ratio analysis of NORSAR long-period P waves, Phys. Earth Planet. Inter. 15, 13 – 27.

Bodin, T., M. Sambridge, H. Tkalčić, P. Arroucau, K. Gallagher, and N. Rawlinson. (2012). Transdimensional inversion of receiver functions and surface wave dispersion. J. Geophys. Res. 117, B02301. doi:10.1029/2011JB008560

Christensen, N. I., and Mooney, W. D., 1995. Seismic velocity structure and composition the continental of crust: A global view. J. Geophys. Res., vol. 100, B7, 9761-9788.

Doherty, J., and J.M. Johnston (2003). Methodologies for calibration and predictive analysis of watershed model, J. Am. Water Resour. Assoc. 39(2), 251–265, doi:10.1111/j.1752-1688.2003.tb04381.x.

Gallagher, M.R., and J. Doherty (2007). Parameter estimation and uncertainty analysis for a watershed model, Environ. Modell. Softw. 22, 1000–1020.

Gallardo, L. A. and Meju M. A. 2003. Characterization of heterogeneous near-surface materials by joint 2D inversion of dc resistivity and seismic data. Geophys. Res. Lett., 30(13), 1658, doi:10.1029/2003GL017370.

Gallardo, L. A. and Meju, M. A. 2007. Joint two-dimensional cross-gradient imaging of magnetotelluric and seismic traveltime data for structural and lithological classification. Geophys. J. Int. 169, 1261–1272.

Julià, J., C.J. Ammon, R.B. Herrmann, and A. M. Correig (2000). Joint inversion of receiver function and surface wave dispersion observations, Geophys. J. Int. 143, 99–112.

Keller, G.V., 1989, Electrical properties, in Carmichael, R.S., ed., Practical handbook of physical properties of rocks and minerals: Boca Raton, Florida, CRC Press, p. 359–427.

Korja, T., 1997. Electrical Conductivity of the Lithosphere - Implications for the Evolution of the Fennoscandian Shield . Geophysica, 33(1), 17-50.

Lawrence, J.F., and D.A. Wiens (2004). Combined Receiver-Function and Surface Wave Phase-Velocity Inversion Using a Niching Genetic Algorithm: Application to Patagonia, Bull. Seismol. Soc. Amer. 94(3), 977-987.

Özalaybey, S, Savage, M.K., Sheehan, A.F., Louie, J.N., Brune, J.N. (1997). Shear-Wave Velocity Structure in the Northern Basin and Range Province from the Combined Analysis of Receiver Functions and Surface Waves , Bull. Seismol. Soc. Amer. 87(1), 183-199.

Simpson, F., and Bahr, K. (2005). Practical Magnetotellurics, 254 pp., Cambridge University Press, Cambridge, UK.

Tarantola, A. (2005). Inverse problem theory and methods for model parameter estimation, Society for Industrial and Applied Mathematics. Philadelphia. 342p.

Tikhonov, A., and Arsenin, V. 1977. Solutions of Ill-Posed Problems, 258 pp., V.H. Winston, Washington, D.C.

Vecchia, A.V., and R.L. Cooley (1987). Simultaneous confidence and prediction intervals for nonlinear regression models with application to a groundwater flow model, Water Resour. Res. 23 (7), 1237-1250.

Zevallos, I., Assumpcao, M. and Padilha, A. I., 2009. Inversion of teleseismic receiver function and magnetotelluric sounding to determine basement depth in the Paraná Basin, SE Brazil. Journal of Applied Geophysics, 68, 231–242.

2. – Uncertainty analysis in the joint inversion of receiver function and surface-wave dispersion, Paraná Basin, southeast Brazil

Lucas P Moreira[1], Michael J. Friedel[2,3] and George S. França[1]

[1] Institute of Geosciences, University of Brasilia, University Campus Darcy Ribeiro, Asa Norte, Brasilia, 70910-900 Brazil

[2] Crustal Imaging and Geochemistry Science Center, United States Geological Survey, Denver Federal Center, Bldg. 20, MS-964, Denver, Colorado 80225, United States

[3] Center for Computational and Mathematical Biology, University of Colorado, Campus Box 170, PO Box 173364, Denver, CO 80217-3364 United States

Submitted to Bulletin of the Seismological Society of America on May 7th, 2012
Accepted for publication on January 24th, 2013
To be published on June, 2013

Abstract

The joint inversion of receiver function and surface-wave dispersion data is popular because it reduces the non-uniqueness of the modeled subsurface seismic velocities. Whereas various inverse procedures have been used in joint subsurface imaging, the evaluation of uncertainties in the estimated parameter distribution is usually overlooked or considered qualitatively. We present a quantitative method for determination of uncertainty in velocity models estimated by the joint inversion of receiver function and surface-wave data by using the prediction of each observation sample to map the objective function surface and create a statistical distribution of estimated model parameters. The proposed methodology is evaluated in a controlled test using synthetic

data simulating a realistic shear wave velocity model. We then apply the method to field data recorded at the POPB seismic station in the Paraná Basin, southeast Brazil. The respective range of uncertainty for modeled S-wave velocity distributions in the synthetic and field tests were 0.111 – 0.412 (2.5-9.2 %) km/s, and 0.110-0.341 km/s (2.5-7.9 %).

2.1 – Introduction

The numerical inverse process used to estimate a seismic velocity model contains uncertainty due to forward modeling errors, data noise, and local minima, especially in cases of non-linearity and high correlation between inverted parameters (Doherty and Johnston, 2003; Julià et al. 2000). Besides being able to qualitatively improve the imaging process (Gallardo and Meju, 2004; Moorkamp et al. 2010), the joint inverse procedure can reduce uncertainties in the estimated velocity structure. Usually the joint inversion of receiver functions (RF) and surface wave dispersion (SWD) is based on linearized methods (Julià et al, 2000), evolutionary algorithms (Lawrence and Wiens 2004, An and Assumpção, 2004) or Bayesian methods (Bodin et al, 2012). The inversion process seeks the model having the minimum difference between predictions from a numerical forward model and field observed data using a least-square minimization scheme (Gallagher and Doherty, 2007a). A velocity model is considered optimal when this function reaches a minimum value. Unfortunately, the estimated velocity model is nonunique; that is, there are an infinite number of parameter combinations which satisfy the objective function (Tarantola, 2005). Therefore, the assessment of different velocity models satisfying the objective function criterion can provide information about the magnitude of the uncertainty in the joint inverse process.

The uncertainties in estimated parameter values are often expressed as confidence levels determined from the model covariance matrix calculated as part of the inversion process (Julià et al, 2000). Unfortunately, this approach assumes linearity and independence of parameters which is not always a good approximation (Gallagher and Doherty, 2007b). An alternative Bayesian approach (Gelman et al, 2004) calculates an *a posteriori* probability distribution of parameter values and their associated uncertainties based on an *a priori* distribution. Such methods can provide a likelihood measure for each inverted velocity value; however, the computational effort can be too high for complex or highly nonlinear joint geophysical models.

In this paper, the aim is to evaluate the efficacy of a nonlinear prediction procedure for determining the magnitude of uncertainty in velocity models (Vecchia and Cooley, 1987; Gallagher and Doherty, 2007a; Friedel, 2011). In this procedure, we hypothesize that estimated models having the same (or very similar) final objective function values are equally valid. The objective is to estimate the statistical distribution of velocities associated with models determined using the joint RF-SWD inverse procedure for synthetic data, and field data collected at the POPB seismic station, Parana, Brazil. By applying the proposed procedure to all velocities in the observed profile, an objective function minimum region can be mapped providing the statistical distribution.

2.2. – Methodology

2.2.1. – Linearized Inversion

The first step associated with analyzing uncertainty in the joint inversion is model estimation; that is, finding a parameter set which characterizes a 1-dimensional (1D) subsurface seismic (S) velocity profile. In this study, we use the Gauss-Marquardt-Levenberg algorithm (see Data and Resources section) based on the objective function negative gradient. In this case, we define a linear system as:

$$\mathbf{X}\,\mathbf{b} = \mathbf{c}, \tag{1}$$

where the constant elements in the *m x n* matrix **X** represent the structural aspects of the model and are independent from vector **b**, a *n*-dimension vector containing the S velocity parameters. **c** is a *m* dimensional vector with the observation samples. The analytical solution of equation (1) depends on the system complexity, so it is solved by minimizing iteratively the function Φ, defined by:

$$\Phi = (\mathbf{c} - \mathbf{X}\mathbf{b})^{t}\mathbf{Q}(\mathbf{c} - \mathbf{X}\mathbf{b}) \tag{2}$$

where **Q** is a *m x m* diagonal matrix with the observation weights (Hill, 1998), and *t* is the transpose of the matrix. Extending this solution to non-linear systems the relationship between the parameters and observations can be expressed as:

$$\mathbf{c} = f(\mathbf{b}) \tag{3}$$

where $f(\ )$ is a function which maps n-dimensional parameter space into m-dimensional observation space, giving the nonquadratic objective function:

$$\Phi = (\mathbf{c} - f(\mathbf{b}))^t \mathbf{Q} (\mathbf{c} - f(\mathbf{b})) \quad (4)$$

This function is minimized iteratively replacing the **X** matrix by the Jacobian matrix **J** with *m* rows (one for each observation), where the *n* elements of each row represents the derivative of one particular observation with respect to each of the *n* parameters, and the equation (1) is re-written as:

$$\mathbf{c} = \mathbf{c}_0 + \mathbf{J}(\mathbf{b} - \mathbf{b}_0). \quad (5)$$

This is a linearization of the non-linear relationship between **c** and **b** using Taylor's theorem, thus the minimization is carried out on the following objective function Φ:

$$\Phi = (\mathbf{c} - \mathbf{c_0} - \mathbf{J}(\mathbf{b} - \mathbf{b_0}))^t \mathbf{Q} (\mathbf{c} - \mathbf{c_0} - \mathbf{J}(\mathbf{b} - \mathbf{b_0})), \quad (6)$$

where the subscript $_0$ represents values calculated by the forward model and vectors without subscripts are the observation values.

Minimization of Φ is conducted by iteratively updating the vector **b** given by:

$$\mathbf{b} - \mathbf{b_0} = (\mathbf{J}^t \mathbf{Q} \mathbf{J})^{-1} \mathbf{J}^t \mathbf{Q} (\mathbf{c} - \mathbf{c}_0). \quad (7)$$

To stabilize the nonlinear inversion process, the Marquardt parameter α is added. Replacing the difference $(\mathbf{b} - \mathbf{b}_0)$ by the update vector **u** gives:

$$\mathbf{u} = (\mathbf{J}^t \mathbf{Q} \mathbf{J} + \alpha \mathbf{I})^{-1} \mathbf{J}^t \mathbf{Q} (\mathbf{c} - \mathbf{c}_0), \quad (8)$$

where α is the Marquardt parameter, and **I** is the *n x n* identity matrix.

The joint inversion of RF and SWD models involves observations with different magnitudes. To handle this, a scaling matrix is introduced, $\mathbf{S}_{ii} = (\mathbf{J}^t\mathbf{Q}\mathbf{J})_{ii}^{-1/2}$, in the previous equation to normalize the Jacobian matrix elements. The equation (8) becomes:

$$\mathbf{S}^{-1}\mathbf{u} = ((\mathbf{JS})^t\mathbf{QJS} + \alpha\mathbf{S}^t\mathbf{S})^{-1}(\mathbf{JS})^t\mathbf{Q}(\mathbf{c} - \mathbf{c}_0), \quad (9)$$

which is mathematically identical to equation (8), but numerically more stable. This procedure is applied iteratively until the value of the objective function reaches a prescribed minimum.

2.2.2. – Prediction

Starting from a previously estimated velocity model, it is possible to find a set of parameters (for example, shear-wave (S-wave) velocities) that maximize (or minimize) a particular observation sample (for example, the RF value at a particular time or a SWD value at a particular period). Under a prediction state, the equation (3) is given by:

$$s = g(\mathbf{b}) \quad , \quad (10)$$

where *s* is the prediction sample (scalar value) replacing the observation vector **c** under the estimation condition.. Under this condition equation (10) can be rewritten in an iterative fashion similarly to equation (5) as:

$$s - s_0 = \mathbf{z}^t(\mathbf{b} - \mathbf{b}_0), \tag{11}$$

where the subscript $_0$ represents the previous iteration and **z** is the sensitivity vector for a model output containing the vector **b** model prediction coefficients, which is an equivalent representation of the linear matrix **J** in equation (5).

The confidence interval of a prediction is defined by the interval between the minimum and maximum prediction that can be made by the model using parameters jointly located in a confidence region defined at a specified probability level (Friedel, 2011). For a non-linear confidence region containing the prediction an approximate region may be obtained using the likelihood ratio method (Vecchia and Cooley, 1987), the solution is defined by:

$$\Phi(\mathbf{b}) - \Phi(\underline{\mathbf{b}}) \leq n\sigma_r^2 F_\alpha(n,m\text{-}n), \tag{12}$$

where $\Phi(\mathbf{b})$ is the objective function for a parameter set **b**, $\Phi(\underline{\mathbf{b}})$ is the nonquadratic objective function calculated from the parameters' optimal values defined by equation (4), $\sigma_r^2 = \Phi(\underline{\mathbf{b}})/(m\text{-}n)$ is the reference variance calculated during the model estimation and F(.) is the F distribution.

For the prediction of a non-linear model, the boundary of the confidence interval can be calculated by minimizing (or maximizing) the prediction *s* in equation (10) while jointly constraining parameter values within the confidence region defined in (12). Using the method of Langrange multipliers, the prediction of nonlinear confidence limits can be calculated using the equation (Cooley and Vecchia, 1987; Vecchia and Cooley 1987):

$$\mathbf{b} - \mathbf{b}_0 = (\mathbf{J}^t\mathbf{Q}\mathbf{J})^{-1}\{\mathbf{J}^t\mathbf{Q}(\boldsymbol{c} - \boldsymbol{c_0}) - \mathbf{z}/2\lambda\}, \quad (13a)$$

where the Lagrange coefficient λ is defined by:

$$\left(\frac{1}{2\lambda}\right) = \pm\left[\frac{\Phi(\underline{\mathbf{b}}) + \delta - (\boldsymbol{c} - \boldsymbol{c_0})^t\mathbf{Q}(\boldsymbol{c} - \boldsymbol{c_0}) + (\boldsymbol{c} - \boldsymbol{c_0})^t\mathbf{Q}\mathbf{J}(\mathbf{J}^t\mathbf{Q}\mathbf{J})^{-1}\mathbf{J}^t\mathbf{Q}(\boldsymbol{c} - \boldsymbol{c_0})}{\mathbf{z}^t(\mathbf{J}^t\mathbf{Q}\mathbf{J})^{-1}\mathbf{z}}\right]^{1/2} \quad (13b)$$

where δ is the right side of equation (12). The system of equations (13) is numerically stable for over-determined problems, requiring that the number of observations *m* must be higher than the number of parameters *n*. It is solved once for the plus sign and once for the minus sign, defining respectively the maximum and the minimum critical values of the prediction sample *s* inside the confidence region. This numerical solution is reached iteratively calculating an upgrade vector (equation 13a) by repeated linearization through the Jacobian matrix calculation.

For example, consider a model with only two parameters p1 and p2. The objective function of this system can be represented by a surface, as in figure 1a, where the gray area represents a minimum region. The joint-inversion process consists of finding the parameter set associated with this region. These nonlinear inversions provide non-unique solutions with parameter combinations (different models) and corresponding objective function values inside the confidence region defined by a model estimation threshold ($\Phi(\underline{\mathbf{b}}) + \delta$). A particular sample will have its value increased (or decreased) in a certain direction as p1 and p2 change, as shown in figure 2.1b. Combining both pictures in figure 2.1c, it is possible to define the critical points, each

one consisting in a set of parameters (p1 and p2), in the objective function surface corresponding to the maximum and minimum values of the predicted observation for a given model.

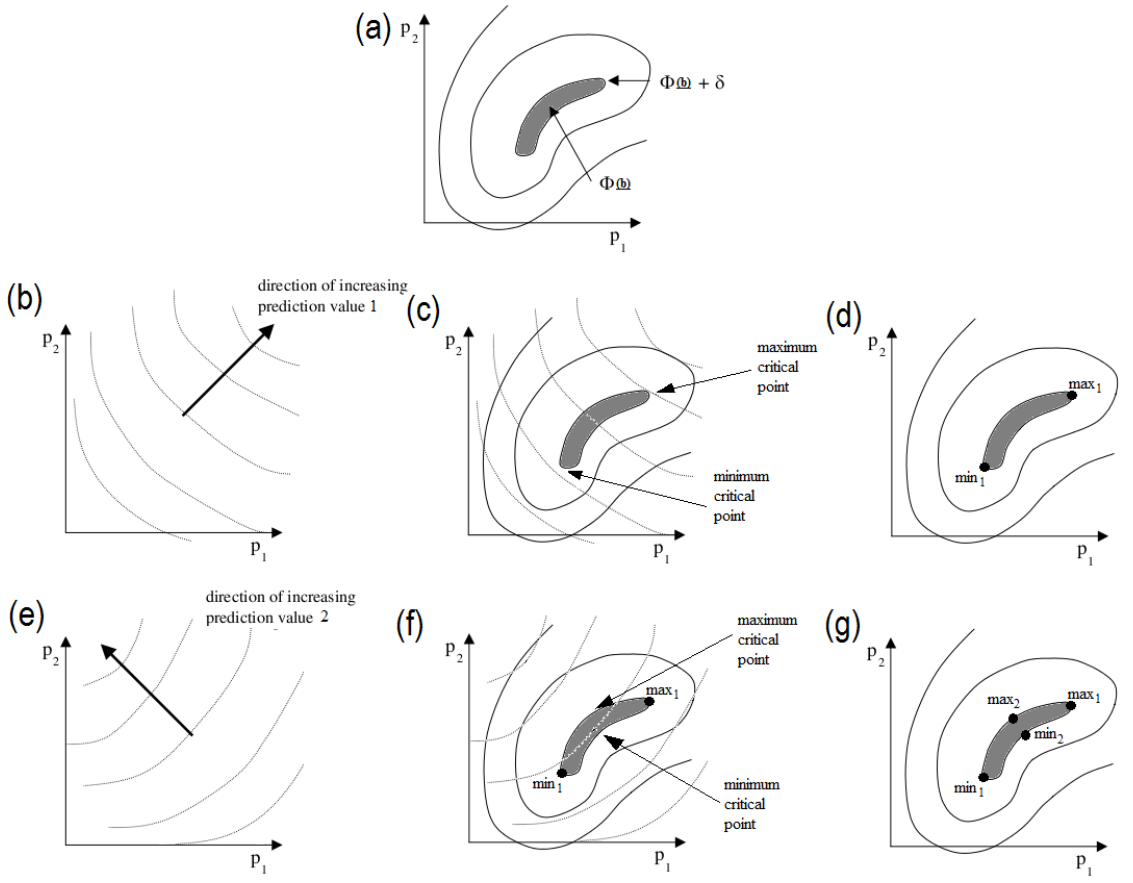

Figure 2.1 – Non-linear system with two model parameters p1 and p2. (a) Objective function surface with a minimum region (gray area) defined as sufficient to consider the model optimal. (b) Increasing direction of one particular observation sample based on parameters variation. (c) Combination of these two pictures (d) showing the maximum and minimum critical values for the estimated model. (e) Increasing direction of other particular observation sample. (f) Maximum and minimum critical values for the second observation. (g) Four critical points representing four model parameter combinations inside the objective function estimation threshold region. (adapted with permission from Doherty, 2005)

The same procedure can then be applied to a different observation providing two more critical points at a different location in the confidence region (gray area) and consequently two more different combinations of parameters values under the model estimation threshold, illustrated by pictures 2.1e to 2.1g. If the number of observations used in the model estimation process is large enough and independent, the above procedure will result in a model set that maps the objective function confidence region and information describing parameters uncertainties. For the joint inversion problem of receiver function and surface waves dispersion curves all observation points are related to the same parameter vector (S-wave velocity), thus each point of the observation samples vector will provide a different confidence interval for the same parameters. In the case of receiver functions, adjacent observation samples in a trace are highly correlated with critical points very close in the objective function surface. By contrast, receiver function observation samples located in different regions in a RF trace represent different sub-surface structures and therefore have distant critical points. In a similar way, surface-wave dispersion samples represent different depths in a seismic velocity profile with non-adjacent samples weakly correlated and critical points distant from each other. Hence, this process is applied to all observations in **c** vector, which leads to *2m* predictions. Therefore, the computational effort to achieve the full solution (critical points population) will depend on the complexity of the inversion problem, the defined confidence interval and the number of observations.

2.3. – Synthetic test

The proposed methodology was tested with data generated using a synthetic

model portrayed in figure 2.2. This model characterizes a 1D S-velocity profile adapted from the IASP91 model (Kennett and Engdahl, 1991) with three layers over a half-space. The abrupt contrasts between each layer contain the main features usually found in crustal modeling using RF and SWD: a sediment layer, the upper and lower crust (containing the Conrad and Moho geological discontinuities), and the upper mantle.

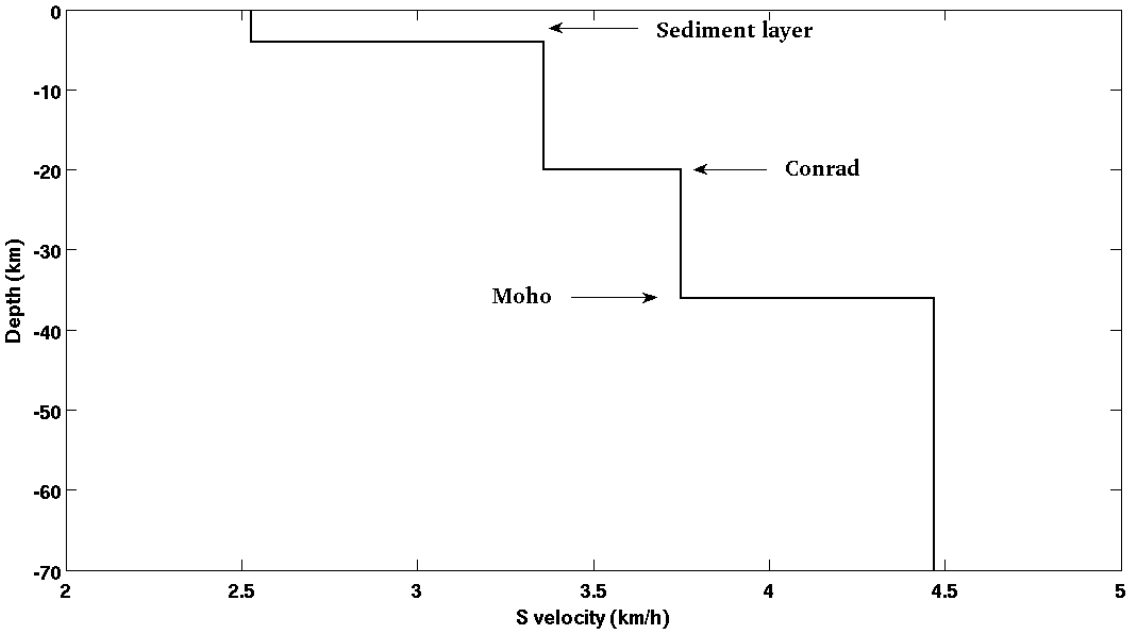

Figure 2.2 – 1D profile used to generate synthetic seismograms used in the joint inversion of receiver function and surface-wave dispersion.

2.3.1. – Receiver functions

To generate synthetic RF traces, we use the Randall algorithm (Randall, 1989) based on Kennett's reflection matrix (Kennett, 1983). This algorithm is selected for its simplicity (low computational effort) and consistent results for models with horizontal and homogeneous layers. Methods available for RF processing include frequency-domain deconvolution (Langston, 1979), time-domain iterative deconvolution (Ligorria

and Ammon, 1999), and the time-domain autoregressive deconvolution (Wu et al, 2007). For high amplitude and high signal-to-noise events, all of these techniques provide similar results. The time-domain methods are not affected by effects introduced by water level equalization (Clayton and Wiggins, 1976) applied in the frequency-domain deconvolution. The iterative time-domain deconvolution is used here due to its stability and relatively rapid processing time.

In crustal modeling, the primary events (P- to S-wave converted phase associated with the Moho discontinuity and multiple reverberations in the crust) comprising a RF trace follow the incident P-wave, typically occurring in the first 30 seconds of a seismogram. To ensure correct representation of crustal features, the simulated RF traces are generated using 60 seconds of record. To simulate realistic field RFs, we also added random noise characterized by a Gaussian distribution and amplitude of 2% of the direct P wave in both seismograms (Moorkamp et al., 2010). The radial components of several seismograms are then deconvolved with the vertical component using the time-domain iterative algorithm (Ligorria and Ammon, 1999) and up to 500 iterations. The resulting RF trace is then truncated 2 seconds before and 30 seconds after the direct P wave resulting in a time series with 400 observation samples. The stack of traces (mean of each time sample) is used as observation data in the inversion process (vector **c,** equation 6) with the inverse of each time sample standard deviation used as observation weights (**Q** matrix, equation 6) (Friedel, 2005). To enhance the joint inverse procedure, the first 20 samples are assigned zero weights because they represent sample information occurring before the direct P-wave.

2.3.2. – Surface wave dispersion

Dispersion curves from both surface-wave group and phase velocities can be obtained; however, the phase-velocity calculation requires that data from an event are recorded by seismic stations located along the same path. Another challenge with SWD is that the horizontal components of seismograms are often affected by higher levels of noise than the vertical component. The presence of noise in the horizontal components makes it difficult to obtain high quality Love-wave dispersion curves especially for long periods. For these reasons, only the fundamental Rayleigh-wave mode group velocities are processed and incorporated into our inversion. For surface waves, the synthetic seismograms and dispersion curve calculations are based on algorithms described in Computer Programs in Seismology (see Data and Resources section). Using these algorithms, we created observations at 20 periods between 20 and 50 seconds. As with RF, 2% random noise was added and the mean of the dispersion curves used as observation data with the standard deviation used to calculate observation weights.

2.3.3. – Joint inversion

The synthetic data generated using the previously described procedures were jointly inverted using the algorithm described in *Linearized Inversion* section. A total of 26 parameter values were estimated, the S-wave velocity for 25 layers with fixed thickness (2 km) and the half-space. In the 1D-forward model, the layers are assumed to be locally horizontal and homogeneous. In the forward model calculations, the P-wave velocity was calculated assuming a fixed Poisson ratio of 0.25 and density calculated using the empirical relation of Berteussen (1977). The initial model was characterized as a single homogeneous layer over a half-space. Figure 2.3 shows the results of the joint inversion including the initial model (dotted), synthetic model (dashed) and

estimated model (solid) for the RF and SWD. In general, depth to the sediment-upper crust, Conrad and Moho discontinuities were all well modeled using the joint-inverse procedure. Whereas the absolute velocity values are in agreement with known values, the differences for the upper crustal layer occurring between 6 and 8 km (about than 2.4%) are slightly greater than for the upper mantle layer (below Moho) between 36 and 40 km (about 1.8%). These results demonstrate the robustness of RF and SWD joint inversion when estimating the S-wave profile.

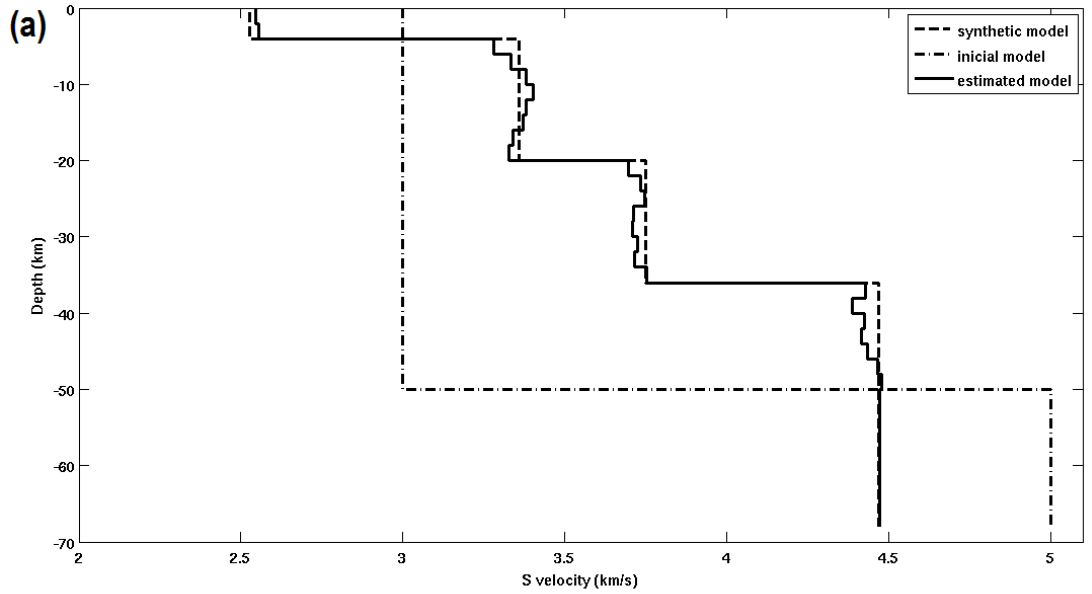
(a)
synthetic model
inicial model
estimated model
Depth (km)
S velocity (km/s)

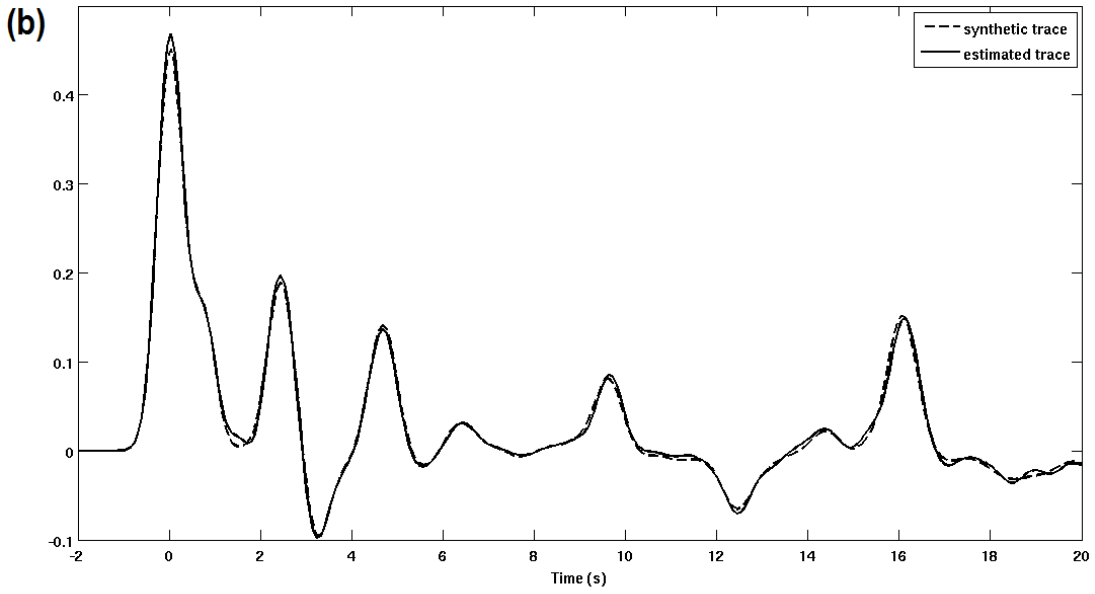
(b)
synthetic trace
estimated trace
Time (s)

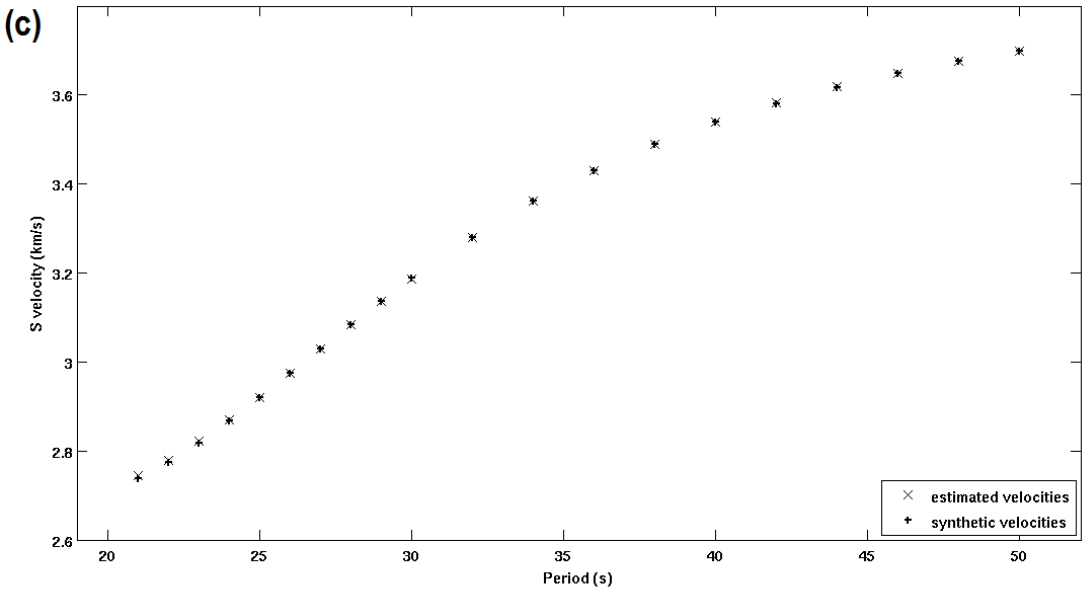
(c)
S velocity (km/s)
estimated velocities
synthetic velocities
Period (s)

Figure 2.3 – (a) RF and SWD joint inversion results. The dashed profile represents the actual (synthetic) model, used to calculate the observation data, the solid profile represents the model estimated by the inversion, and the dotted profile is the inversion initial model. (b) RF traces of the synthetic model (dashed) and the trace from the estimated model (solid). (c) Dispersion curves of synthetic model (pluses) and from the estimated model (crosses).

2.3.4. – Observation prediction and uncertainty analysis

The prediction analysis procedure of Vecchia and Cooley (1987), as described in the *Prediction* section, was applied to all RF and SWD observations having non-zero weights, with a confidence level of 0.99 (equation 12). Estimates of minima and maxima for 275 observation samples (255 RF and 20 SWD samples) resulted in 550 different critical points (1D models) for quantifying the range of S-wave uncertainty with depth. Examples of different critical points location (predicted 1D S-velocity model) on the objective function minimum contour for 3 non-adjacent RF observation samples (numbers 54, 86, and 226) are shown in figure 2.4. Inspection of this figure reveals nonlinear relations among uncertainty associated with different observations. The mapping of all possible observation samples minima and maxima are shown in figure 2.5, where each 1D model is one critical point calculated by the prediction procedure. Notice that some layers show S-wave values that are asymmetrically distributed around the initial value (estimated model). This nonlinear relation in parameter uncertainty suggests that using linear statistics may lead to an inappropriate velocity interpretation.

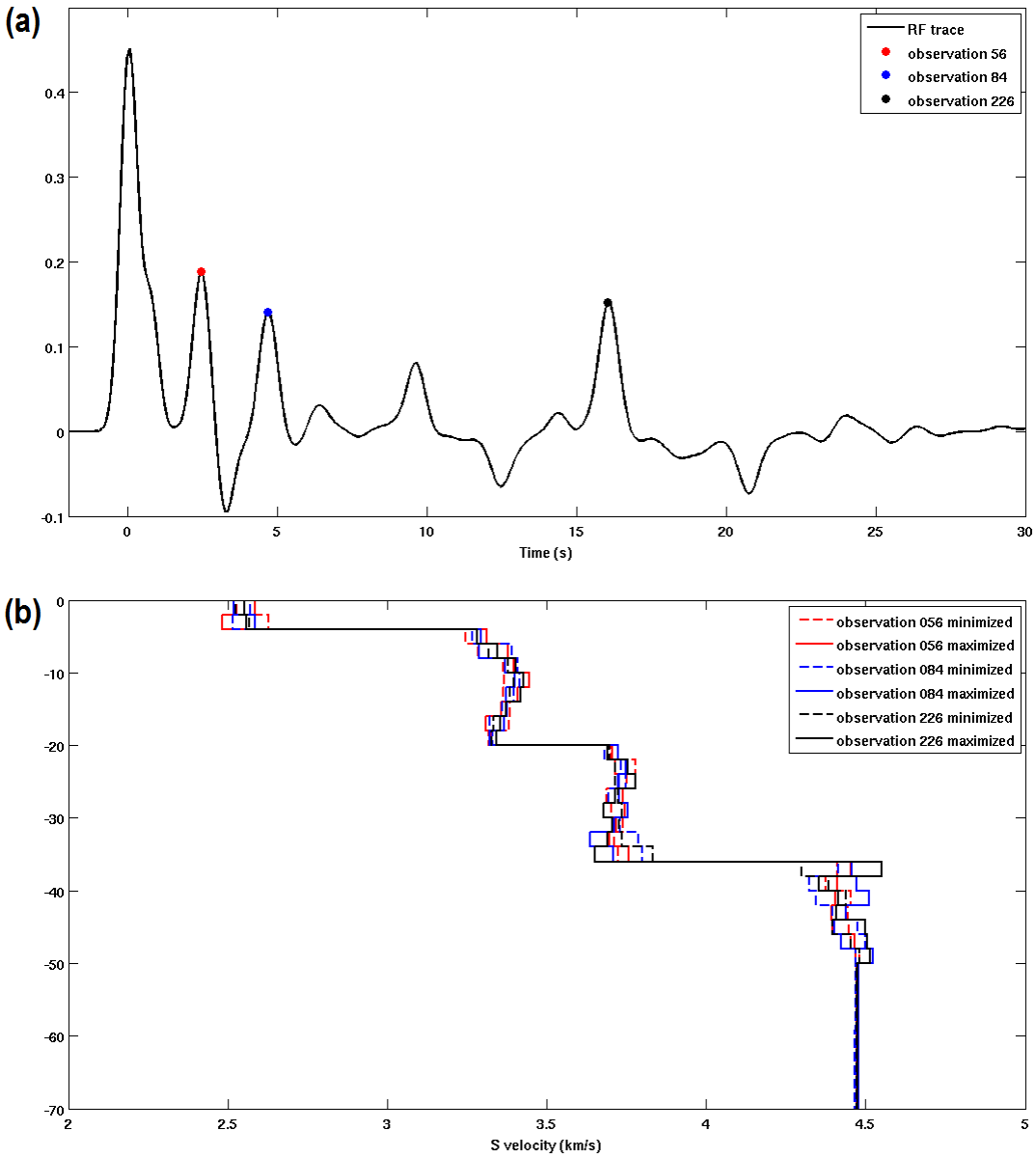

Figure 2.4 – (a) RF trace and three observation samples (54, 86, 224) occurring at different time locations, (b) one-dimensional S-velocity profile obtained by maximizing (dotted lines) and minimizing (dashed lines) the 3 observation samples in (a).

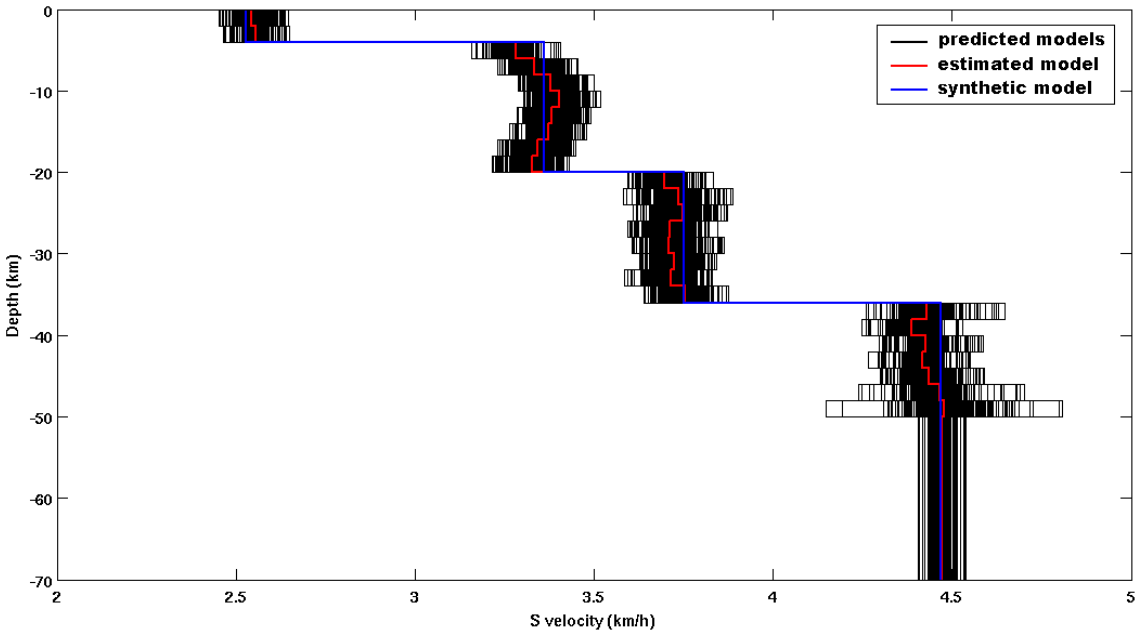

Figure 2.5 – One-dimensional S-velocity profiles obtained from each observation sample prediction (black), profile estimated by the joint inversion (red), and model used to build the synthetic observation data (blue).

A more appropriate description of the confidence interval for the velocity can be obtained by fitting a statistical distribution to the collection of critical values for each layer. Some distributions were tested for selected layers (Figure 2.6), above and adjacent to the sediment discontinuity (layer 2), below and adjacent to the Conrad discontinuity (layer 11), below and adjacent to the Moho (layer 19), showing Normal, t location-scale and logistical distributions fit to the data; the t location-scale and/or logistic fit better than normal, resulting in improved S-wave velocity uncertainty assessment. While the fitted distributions are symmetric and have similar shape to a normal distribution, the mean (or median) values differ from the estimated values determined in the joint-inverse procedure. This shows that the range of possible values for a certain layer is not equally distributed around the estimated value. Figure 2.7 shows the estimated model and related profiles corresponding to quantiles calculated

using the critical values. The limits for each quantile represent the percentage of models obtained by the prediction that are contained in each percentile range providing a statistical range of values for a defined confident interval, differing from Bayesian approach which provides the uncertainties as a probability density function for each inverted parameter. These results can be used as a practical measure of possible parameter values for each layer assuming that the estimated model is correct. For example, at the 95th percentile, the predicted range of velocity in the upper mantle (layer between 48 and 50 km depth) is 0.281 km/s whereas the predicted range of velocity in the sediment (layer between 2 and 4 km depth) is 0.121 km/s.

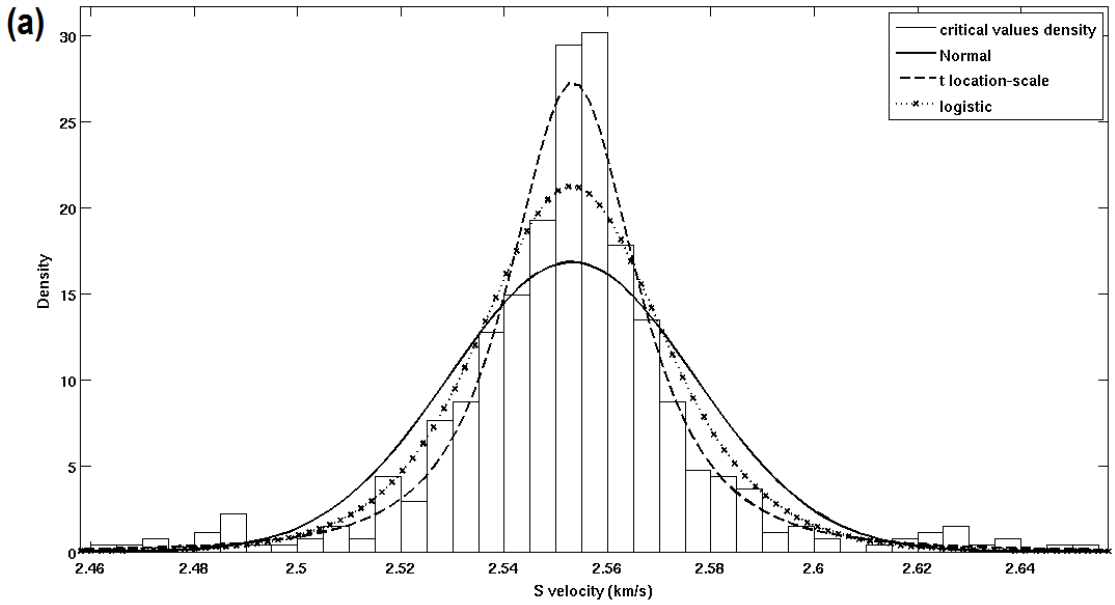
(a)
critical values density
Normal
t location-scale
logistic
Density
S velocity (km/s)
0
5
10
15
20
25
30
2.46
2.48
2.5
2.52
2.54
2.56
2.58
2.6
2.62
2.64

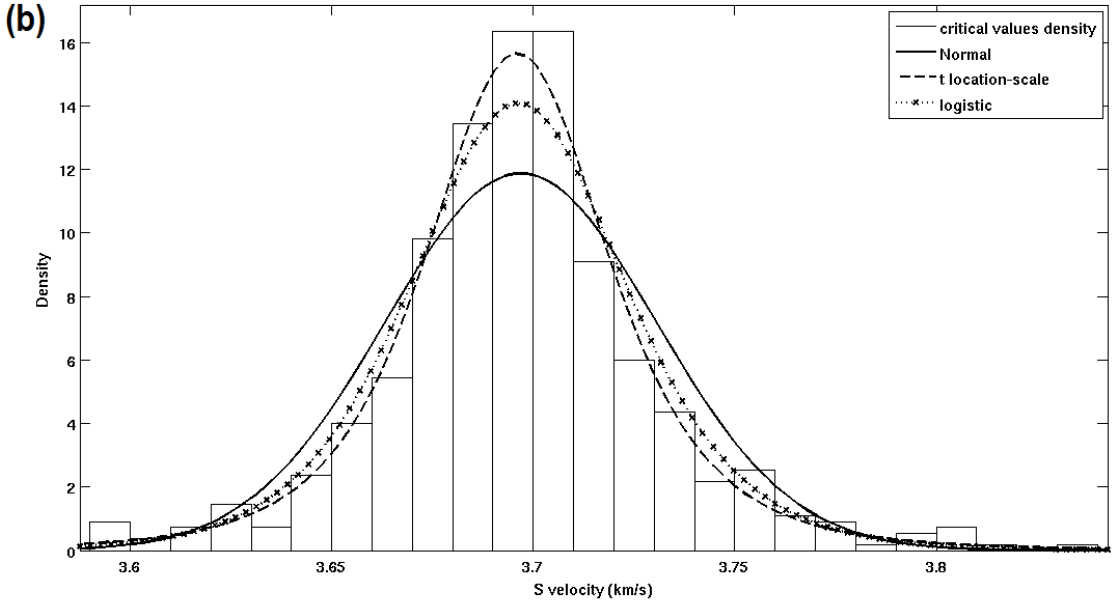
(b)
critical values density
Normal
t location-scale
logistic
Density
S velocity (km/s)
0
2
4
6
8
10
12
14
16
3.6
3.65
3.7
3.75
3.8

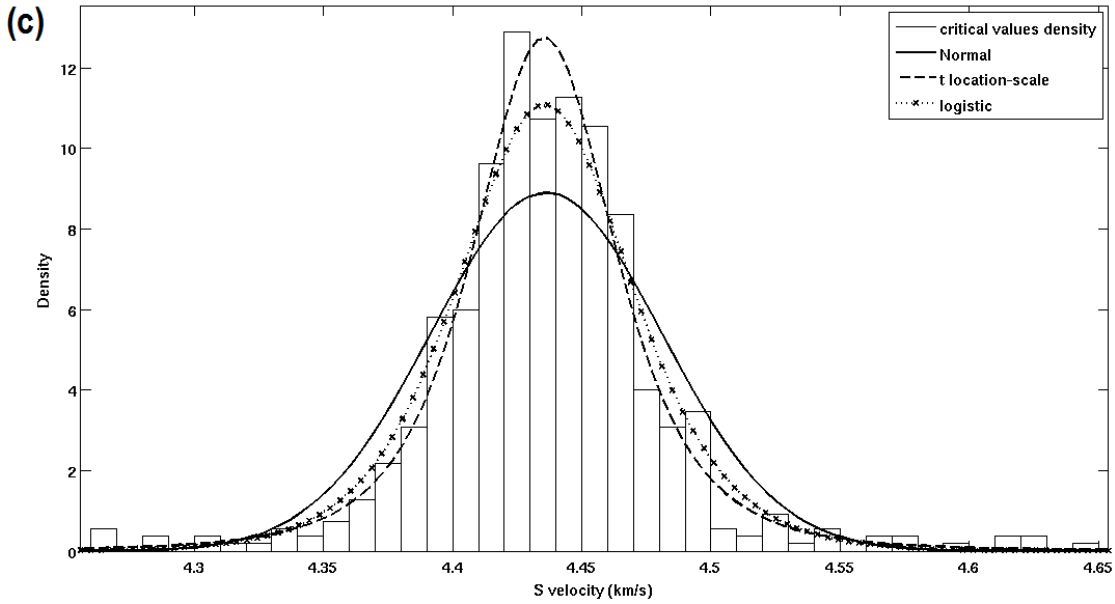
(c)
critical values density
Normal
t location-scale
logistic
Density
S velocity (km/s)
0
2
4
6
8
10
12
4.3
4.35
4.4
4.45
4.5
4.55
4.6
4.65

Figure 2.6 – Probability density functions and statistical distributions that best fit the predicted values for (a) the second layer (b) the layer just below the Conrad discontinuity, and (c) the layer just below Moho.

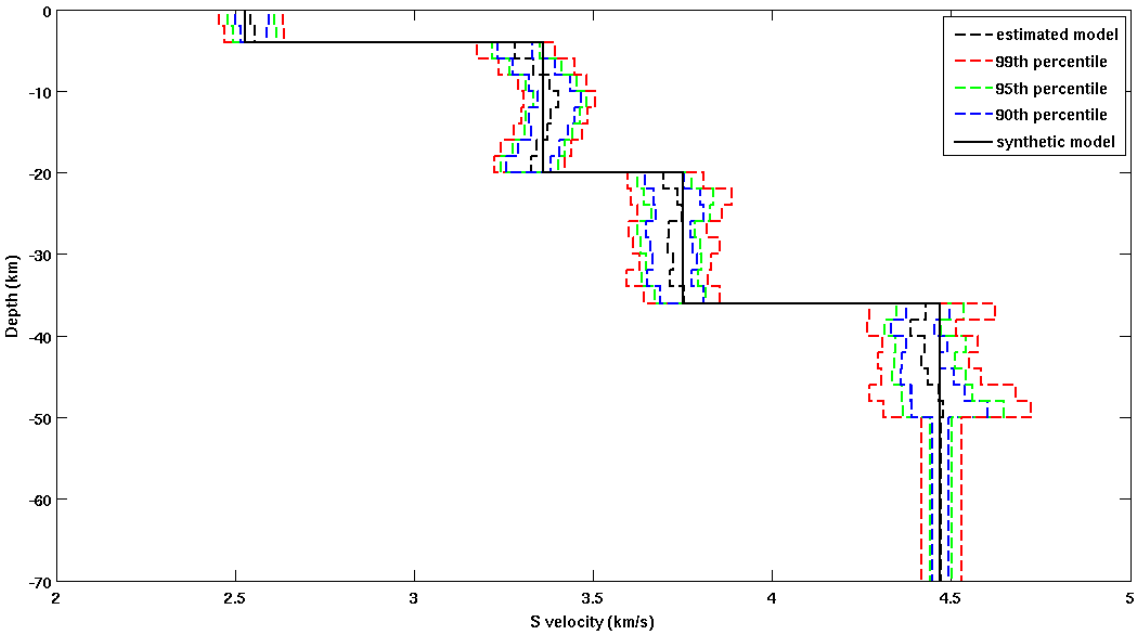

Figure 2.7 – Uncertainty in the estimated S-wave velocity profile (solid black line) including three prediction percentiles: 90th (dashed blue), 95th (dashed green), and 99th (dashed red).

2.4. – Application to field data

The proposed prediction method is applied to field data collected at the POPB seismic station (22.4565ºS, 52.8368ºW), part of the Brazilian Lithospheric Seismic Project (BLSP) located in the Paraná Basin, southeast Brazil. The crustal structure is well studied with geophysical results published by several authors (Assumpção et al. 2002, Assumpção et al., 2004, Snoke & James 1997, An & Assumpção 2006, Juliá et al. 2008).

The surface-wave dispersion curves are taken from Feng et al. (2004) and only samples between 20 and 50 seconds of each curve were used (13 samples per curve) in the joint inversion. RF traces were calculated using the time-domain iterative method (Ligorria and Ammon, 1999) for 6 teleseismic events listed in Table 2.1 containing 320 samples for each trace with 0.1 second of sampling period. The mean of the traces (stack) was used for observation values (vector **c** in equation 6) and the standard deviation for each time sample was used to compose the observation weight matrix, Q in equation (6) (Hill, 1998). Figure 2.8 shows the traces of each event and stack trace. These data were jointly inverted using the global model of IASP91 (Kennett and Engdahl, 1991) as the initial starting model values and the forward model calculations used in the controlled tests (*Joint Inversion* section). Convergence to the estimated model took 18 iterations (Figure 2.9) and is similar to results published by Juliá et al. (2008) and An & Assumpção (2004). This velocity model has three main seismic discontinuities: one between the sediment layer and upper crust at about a 2 km depth, the Conrad discontinuity at about a 12 km depth, and the Moho at about a 43 km depth.

Table 2.1 – Earthquake data used to estimate crustal velocity structure. Waveforms were obtained from the IRIS Data Management Center earthquake datacenter.

Date	Origin time (UTC)	Lat (ºS)	Long (ºW)	Depth (km)	Mag (MW)	BAz (º)
28 Aug 1999	12:40:06.1	1.29	77.55	196.4	6.3	303.579
21 Aug 2000	09:16:25.4	53.02	45.97	10.0	6.1	171.955
28 Sep 2000	23:23:43.3	0.22	80.58	22.9	6.4	305.435
4 Oct 2000	14:37:44.1	11.12	62.56	110.3	6.1	343.178
8 Nov 2000	06:59:58.8	7.04	77.83	17.0	6.5	317.364
31 Jul 2002	00:16:44.6	7.93	82.79	10.0	6.5	302.430

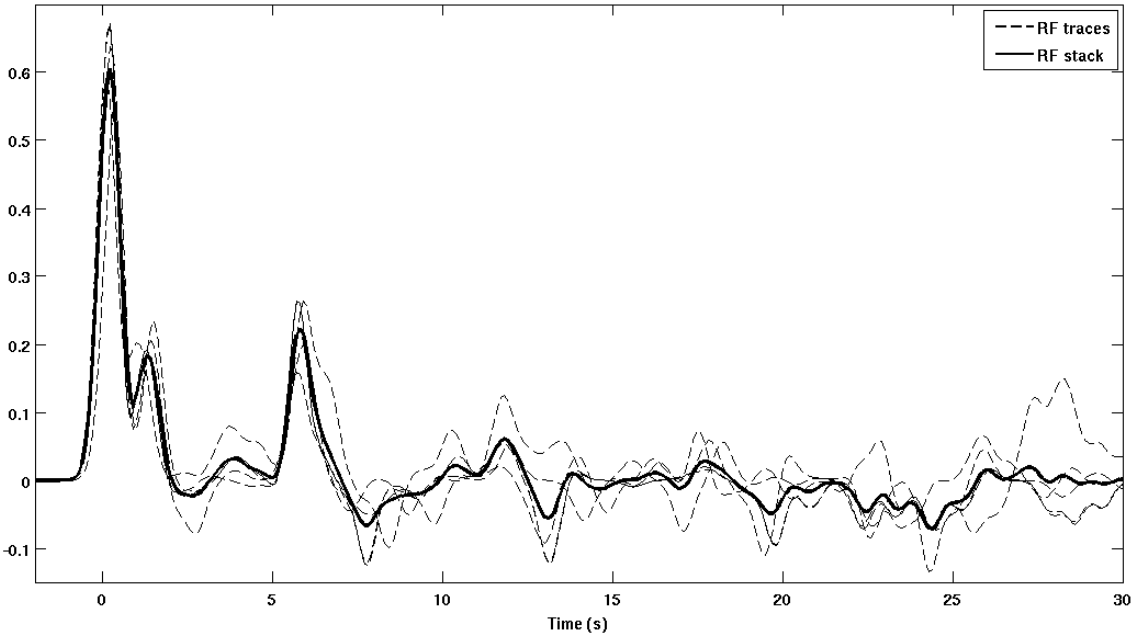

Figure 2.8 – RF traces calculated with the time-domain deconvolution for 6 teleseismic events recorded by POPB station (dashed lines), and the stacked trace (solid line) used as observation samples in the joint-inversion process (vector **c** in equation 2.4)

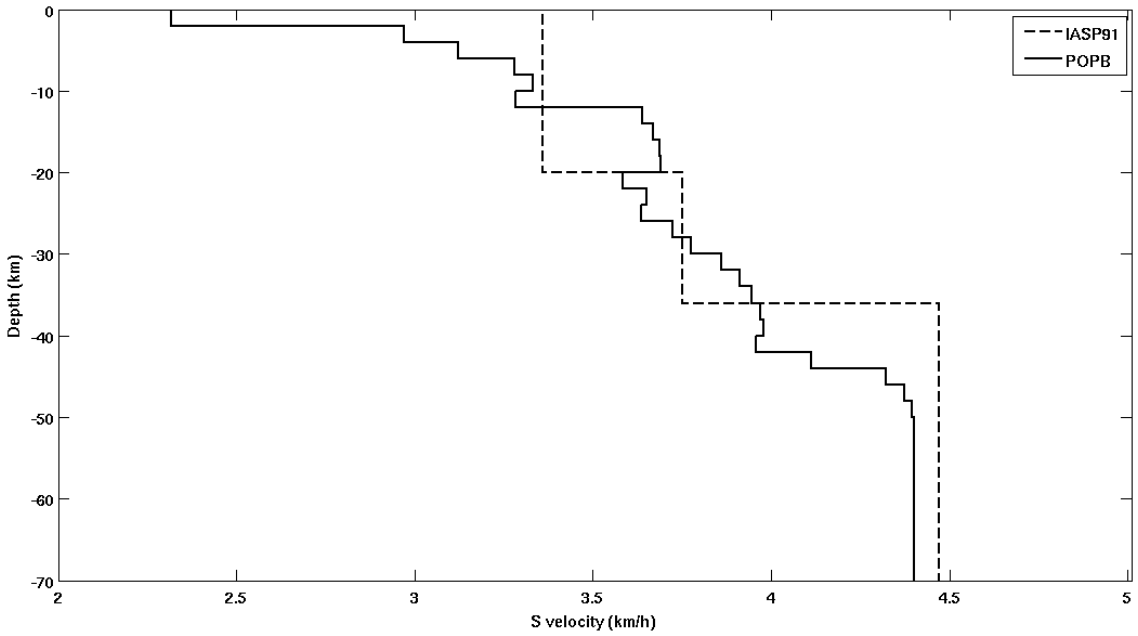

Figure 2.9 – Global model IASP91 (dashed) used as initial values in the joint inversion process and the estimated model (solid) showing three main discontinuities: sediment-upper crust, Conrad and Moho, with depths different from the global model.

Assuming the estimated velocity model is correct, the prediction of each observation sample was applied (maximum/minimum) with a confidence level of 0.99 and critical points over the objective function surface obtained. A total of 626 velocity models were identified that maintained optimal conditions of the estimated model requiring approximately $2x10^5$ forward model calculations, less than half of typical global search procedures (Bodin et al, 2012). The predicted profiles and their quantiles are summarized in figure 2.10. At the 95th percentile, the greatest range of prediction uncertainty (0.23 km/s) was associated with the upper mantle (below the Moho) with less uncertainty in velocity estimates for the crust (0.18 km/s), between 6 and 8 km/s. The smallest magnitude in estimated uncertainty (0.094 km/s) was observed at depths between 18 and 20 km. The modeled estimates for this layer are similar to those provided by Juliá et al. (2008), who used velocity variations between joint inverse models for each receiver function group.

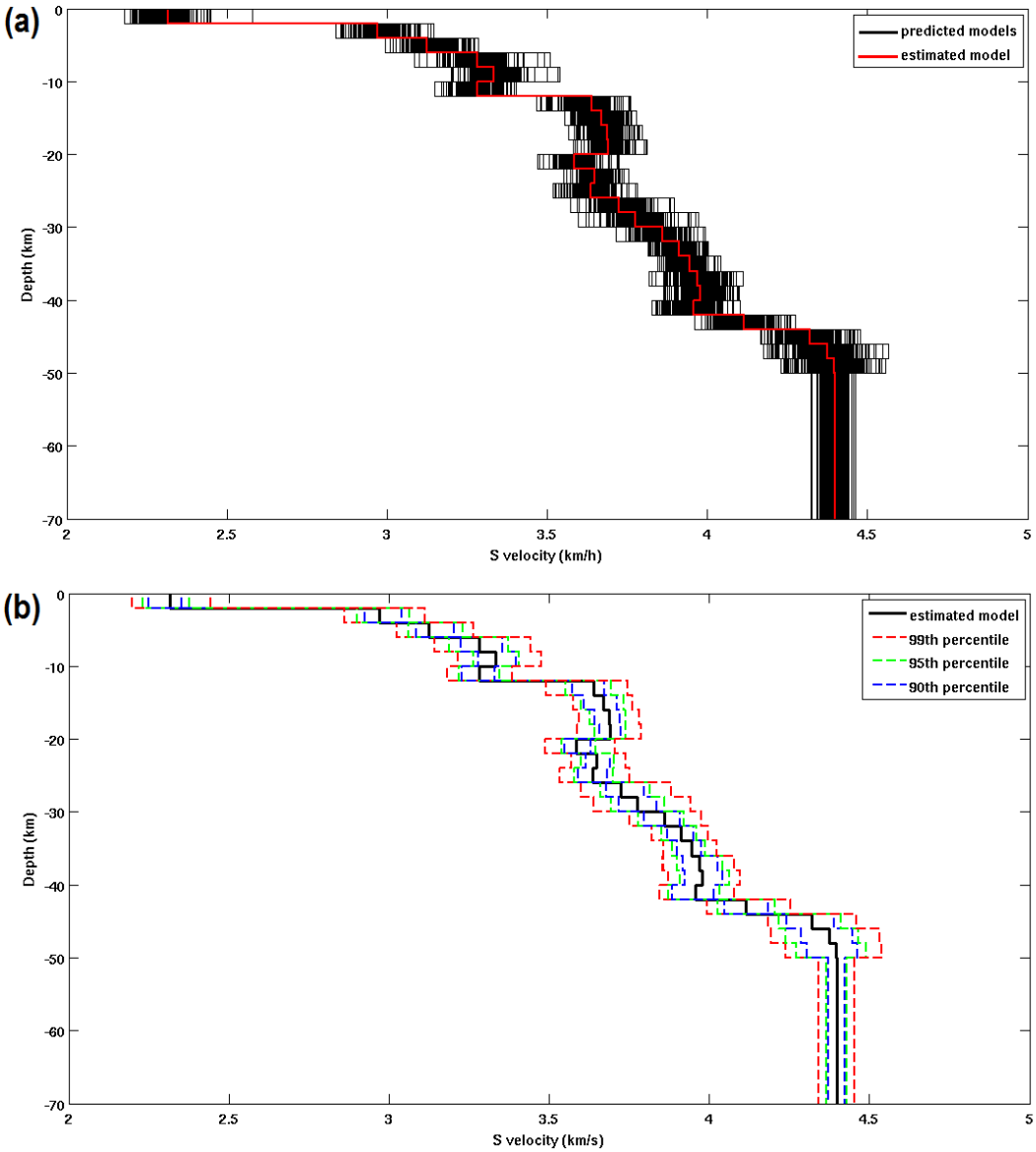

Figure 2.10 – (a) Predicted models for each observation sample (black) and the inversion estimated model (red). (b) Estimated model (solid black line) and the profiles corresponding to the range of percentiles: 90th (dashed blue), 95th (dashed green) and 99th (dashed red) calculated from predicted values.

2.5. – Conclusions

This study successfully demonstrates a novel method for quantifying nonlinear uncertainty in the joint inversion of receiver function and surface-wave dispersion data.

By estimating the maximum and minimum prediction values for all observation samples of a previously estimated velocity model, the statistical information of critical points mapped across an objective function surface can be used to determine conditional quantiles of the inverted parameters. The proposed method is tested using synthetic data and then successfully applied to field data recorded by the POPB seismic station installed in the Paraná basin, southeast Brazil. The similarity of velocity uncertainty estimated in this study to previous studies supports its application in future studies.

2.6. – Data and Resources

All data used in this paper came from published sources. POPB station seismograms used in this study were collected as part of the Brazilian Lithospheric Seismic Project (BLSP) (James *et al.*, 1993). Data can be obtained from the IRIS Data Management Center at *www.iris.edu* (last accessed January 2013). Surface waves dispersion curves are courtesy of Feng Mei (Feng *et al.*, 2004). Computer software package for forward model calculation is encapsulated in Computer Programs in Seismology provided by C. Ammon and R. Herrmann upon request at *http://www.eas.slu.edu/eqc/eqccps.html* (last accessed January 2013). Inversion and prediction algorithms are encapsulated in Parameter Estimation (PEST) package provided by John Doherty at *www.pesthomepage.org* (last accessed June 2012). Some figures were created using Matrix Laboratory (MATLAB, *www.mathworks.com*, last accessed June 2011).

2.7. – Acknowledgements

We specially thank Feng Mei and Marcelo Assumpção for the surface-wave dispersion curves and Burke Minsley for revising the manuscript. LM was fully supported by CAPES and CAPES/Fulbright 23038.034805/2009-71 grants.

2.8. – References

An, M., and M.S. Assumpção (2004). Multi-objective inversion of surface waves and receiver functions by competent genetic algorithm applied to the crustal structure of the Parana Basin, SE Brazil, *Geophys. Res. Lett.* **31**, L05615, doi:10.1029/2003GL019179.

An, M., and M.S. Assumpção (2006). Crustal and upper mantle structure in intracratonic Paraná Basin, SE Brazil, from surface wave dispersion using genetic algorithm. *J. South Amer. Earth Sci.* **21**, 173-184.

Assumpção, M.S., D.E. James, and J.A. Snoke (2002). Crustal thicknesses in SE Brazilian shield by receiver function analysis: implications for isostatic compensation, *J. Geophys. Res.* **107**(B1). doi: 10.1029/2001JB000422.

Assumpção, M., M. An, M. Bianchi, G. S. L. França, M. Rocha, J. R. Barbosa, and J. Berrocal (2004). Seismic studies of the Brasília fold belt at the western border of the São Francisco Craton, Central Brazil, using receiver function, surface-wave dispersion and teleseismic tomography, *Tectonophysics* **388**, 173 - 185

Bodin, T., M. Sambridge, H. Tkalčić, P. Arroucau, K. Gallagher, and N. Rawlinson. (2012). Transdimensional inversion of receiver functions and surface wave dispersion. *J. Geophys. Res.* **117**, B02301. doi:10.1029/2011JB008560

Berteussen, K. A. (1977). Moho depth determinations based on spectral ratio analysis of NORSAR long-period P waves, *Phys. Earth Planet. Inter.* **15**, 13 – 27.

Clayton, R.W., and R.A. Wiggins (1976). Source shape estimation and deconvolution of teleseismic body waves, *J. R. Astr. Soc.* **47**, 151- 177 .

Cooley, R.L., and A.V. Vecchia (1987). Calculation of nonlinear confidence and prediction intervals for ground-water flow models. *Water Resources Bulletin* **23** (4), 581-599.

Dziewonski, A., S. Bloch, and M. Landisman (1969). A technique for the analysis of transient seismic signals, *Bull. Seismol. Soc. Amer.* **59**(1), 427-444.

Doherty, J., and J.M. Johnston (2003). Methodologies for calibration and predictive analysis of watershed model, *J. Am. Water Resour. Assoc.* **39**(2), 251–265, doi:10.1111/j.1752-1688.2003.tb04381.x.

Du Z., G.R. Fouger, B.R. Julian, R.M. Allen, G. Nolet, W.J. Morgan, B.H. Bergsson, P. Erlendsson, S. Jakobsdottir, S. Ragnarsson, R. Stefansson, and K. Vogfjord (2002). Crustal structure beneath western and eastern Iceland from surface waves and receiver functions, *Geophys. J. Int.* **149**, 349–363.

Feng, M., M.S. Assumpção, and S. Van der Lee (2004). Group-velocity tomography and lithospheric S-velocity structure of the South American continent, *Phys. Earth Planet. Inter.* **147**, 315-331.

Friedel, M.J. (2011). A data-driven approach for modeling post-fire debris-flow volumes and their uncertainty, *Environ. Modell. Softw*. Corrected Proof, Available online 30 August 2011.

Friedel, M.J. (2005). *Coupled inverse modeling of vadose zone water, heat, and solute transport: calibration constraints, parameter nonuniqueness, and predictive uncertainty*, *Journal of Hydrology* **312**/1-4, 148-175.

Gallagher, M.R., and J. Doherty (2007a). Parameter estimation and uncertainty analysis for a watershed model, *Environ. Modell. Softw*. **22**, 1000–1020.

Gallagher, M.R., and J. Doherty (2007b). Parameter interdependence and uncertainty induced by lumping in a hydrologic model, *Water Resour. Res.* **43**, W05421, doi:10.1029/2006WR005347.

Gallardo, L.A., and M.A. Meju, (2004). Joint two-dimensional DC resistivity and seismic travel time inversion with cross-gradients constraints, *J. Geophys. Res.* **109**, B03311, doi:10.1029/2003JB002716.

Gelman, A., J.B. Carlin, H.S. Stren, and D.B. Rubin (2004). *Bayesian Data Analysis*

Chapman and Hall, London.

Hill, M.C. (1998). Methods and Guidelines for Effective Model Calibration *U.S. Geological Survey Water-Resources Investigations* Report 98-4005

James, D.E., M. Assumpção, A. Snoke, L.C. Ribotta, and R. Kuehnel (1993). Seismic studies of continental lithosphere beneath SE Brazil, *An. Acad. Bras. Cienc.* **65**(Suppl. 2), 227 – 250

Julià, J., C.J. Ammon, R.B. Herrmann, and A. M. Correig (2000). Joint inversion of receiver function and surface wave dispersion observations, *Geophys. J. Int.* **143**, 99–112.

Julià, J., C.J. Ammon, and R.B. Herrmann (2003). Lithospheric structure of the Arabian Shield from the joint inversion of receiver functions and surface-wave group velocities, *Tectonophysics* **371**, 1 – 21. doi:10.1016/S0040-1951(03)00196-3.

Julià, J., M. Assumpção, and M.P. Rocha (2008). Deep crustal structure of the Parana Basin from receiver functions and Rayleigh-wave dispersion: Evidence for a fragmented cratonic root, *J. Geophys. Res.* **113**, B08318, doi:10.1029/2007JB005374.

Kennett, B.L.N. (1983). *Seismic Wave Propagation in Stratified Media*, Cambridge University Press, Cambridge, England, 342p.

Kennett, B.L.N., and E.R. Engdahl, (1991). Traveltimes for global earthquake location

and phase identification, *Geophys. J. Int.* **105**, 429–465.

Langston, C.A. (1979). Structure under Mount Rainier, Washington, inferred from teleseismic body waves, *J. Geophys. Res.* **84**, 4749–4762.

Lawrence, J.F., and D.A. Wiens (2004). Combined Receiver-Function and Surface Wave Phase-Velocity Inversion Using a Niching Genetic Algorithm: Application to Patagonia, *Bull. Seismol. Soc. Amer.* **94**(3), 977-987.

Li, Y., Q. Wu, R. Zhang, X. Tian, and R. Zeng (2008). The crust and upper mantle structure beneath Yunnan from joint inversion of receiver functions and Rayleigh wave dispersion data, *Phys. Earth Planet. Inter.* **170**, 134-146.

Ligorria, J.P., and C.J. Ammon (1999). Iterative deconvolution and receiver-function estimation, *Bull. Seismol. Soc. Am.* **89**(5), 1395–1400.

Moorkamp, M., A.G. Jones, and S. Fishwick, (2010). Joint inversion of receiver functions, surface wave dispersion,and magnetotelluric data, *J. Geophys. Res*. **115**, B04318, doi:10.1029/2009JB006369.

Poeter, E.P., M.C. Hill, E.R. Banta, S. Mehl, and S. Christensen (2005). UCODE_2005 and Six Other Computer Codes for Universal Sensitivity Analysis, Calibration, and Uncertainty Evaluation. http://www.mines.edu/igwmc/freeware/ucode/.

Randall, G.E. (1989). Efficient calculation of differential seismograms for lithospheric

receiver functions, *Geophys. J. Int.* **99**, 469–481.

Snoke, J. A., and D. E. James (1997). Lithospheric structure of the Chaco and Paraná basins of South America from surface-wave inversion, *J. Geophys. Res.* **102**, 2939–2951.

Tarantola, A. (2005). Inverse problem theory and methods for model parameter estimation, *Society for Industrial and Applied Mathematics*. Philadelphia. 342p.

Vecchia, A.V., and R.L. Cooley (1987). Simultaneous confidence and prediction intervals for nonlinear regression models with application to a groundwater flow model, *Water Resour. Res.* **23** (7), 1237-1250.

Wu, Q, Y. Li, R. Zhang, and R. Zeng (2007). Receiver Functions from Autoregressive Deconvolution, *Pure appl. Geophys*. **164**, 2175–2192.

3. – Joint inversion of receiver function, surface wave dispersion, and magnetotelluric data for 2D crustal modeling

Lucas P Moreira[1], Michael J. Friedel[2,3] and George S. França[1]

[1] Institute of Geosciences, University of Brasilia, University Campus Darcy Ribeiro, Asa Norte, Brasilia, 70910-900 Brazil

[2] Crustal Imaging and Geochemistry Science Center, United States Geological Survey, Denver Federal Center, Bldg. 20, MS-964, Denver, Colorado 80225, United States

[3] Center for Computational and Mathematical Biology, University of Colorado, Campus Box 170, PO Box 173364, Denver, CO 80217-3364 United States

Submitted to Journal of Applied Geophysics on February 26th, 2013

Abstract

A joint inverse scheme is presented to integrate earthquake seismic (receiver function and Rayleigh wave dispersion) and magnetotelluric (electric and magnetic field) data for improved crustal imaging. The proposed methodology uses a Gauss-Marquardt-Levenberg algorithm to minimize a multi-component objective function (differences between estimated and observed receiver function trace, surface wave dispersion curves and magnetotelluric resistivity and phase measurements) with a cross-gradient constraint (differences among adjacent resistivity and seismic velocity parameters). The methodology is evaluated using synthetic data from three 1D seismic models co-located with a 2D magnetotelluric model grid with crustal features including a sedimentary basin, the Conrad discontinuity (boundary between upper and lower crust), and the

Mohorovicic (boundary between the Earth's crust and mantle) discontinuity. Results of the joint inversion show improved resolution in the estimated resistivity structure compared to the traditional inversion of resistivity parameters using only magnetotelluric data. Improvements include resolving lateral variations and depth of discontinuities, and a high-resistivity zone underlying a high-conductivity zone (500-fold contrast). For the seismic 1D models, the absolute values of layer shear-wave velocity are closer (+/-3%) to the synthetic model crustal structures demonstrating benefits of the joint inversion.

3.1. – Introduction

In crustal imaging, the inversion of multiple geophysical data types has become popular. Combining several types of data collected over the same region can potentially reduce ambiguity and enhance inversion results. For example, Meju et al. (2003) analyzed independent electromagnetic and seismic refraction inversions for two-dimensional (2D) models. By inverting each data set individually, the recovered physical property models can be inconsistent with prior knowledge regarding relationships. Cooperative strategies can be employed to ensure consistency between the different models (Bedrosian et al., 2007), but the models obtained are likely to be biased towards the result of the first inversion or the survey with greater sensitivity. Another approach is to fit data sets simultaneously in a joint inversion.

Several investigators perform joint inversions of data from different surveys sensitive to the same physical property. For example, the joint inversion of Rayleigh and Love (surface) wave dispersion data (Ritzwoller and Levshin, 1998; Pasyanos et al., 2001; Mei et al., 2004), and receiver function (RF) and Rayleigh wave dispersion data

has been successful in imaging crustal discontinuities based on seismic velocity (An and Assumpção, 2004; Bodin et al., 2012). Recently, Moreira et al. (2013) demonstrated the benefits of using the joint inverse approach with RF and surface wave dispersion data to reduce uncertainty when imaging crustal discontinuities. Other researchers jointly inverted data sets responsive to different physical properties between which there is an analytic relationship (Zevallos et al., 2009). An empirical equation relating parameters are not always available, especially for crustal soundings with high contrast heterogeneities (e.g. crust-mantle discontinuities).

Fewer work has focused on the joint inversion of disparate data sets where there is no analytic relationship available between the properties. In this case, some investigators found that a numerical constraint geometrically relating the structural distribution of different parameters can be useful. For example, Gallardo and Meju (2007) applied a joint inversion of seismic refraction and magnetotelluric (MT) data in a linearized scheme requiring the co-location of soundings. In other studies, Moorkamp et al. (2007) and Zevallos et al. (2009) jointly inverted RF and MT data for 1D models using methods based on genetic algorithm (GA). More recently, Moorkamp et al. (2010) added surface wave dispersion to the RF and MT 1D joint inversion.

In this study, our aim is to evaluate the usefulness of inverting disparate and multidimensional geophysical data for improved crustal imaging. The objective is to quantify improvements associated with two-dimensional (2D) geophysical imaging of the Moho and crustal structures based on simultaneous integration of receiver function, fundamental mode Rayleigh dispersion, and MT data. This approach extends the joint inverse work of Moreira et al. (2013) who sought to reduce model nonuniqueness and uncertainty by integrating 1D RF and surface wave dispersion data, and Gallardo et al. (2004, 2007) who used the cross-gradient structural constraint to relate two physical

parameters in a single multi-component objective function. Performance of the proposed methodology is validated using data from a synthetic model.

3.2. – Methodology

3.2.1. – Forward model

3.2.1.1. – Receiver function

The RF reflects the subsurface response to body waves crossing geologic structures near to a seismic station. The equation for a RF is defined by the time-domain trace corresponding to the deconvolution:

$$RF(\omega) = R(\omega) / Z(\omega) \quad (1)$$

where $R(\omega)$ and $Z(\omega)$ are the radial and vertical components respectively of a teleseismic waveform expressed in the frequency domain.

This method is convenient for crustal imaging because it mathematically removes source and receiver instrument effects from the seismogram (Ammon, 1991). The processing scheme is done through deconvolution of the radial and transverse components using the vertical component. This process results in a time series comprising linear combinations of peaks representing refraction and reflections of body waves through a velocity discontinuity. Part of the energy crossing the discontinuity is converted from compressional (P) to shear (S) waves and vice-versa (Aki and Richards,

1980). As they have different propagation velocities, these phases reach the station in different times and are represented in the RF trace as time shifted peaks, making possible the subsurface imaging of seismic velocity.

A primary characteristic of the RF trace is its sensitivity to seismic velocity contrasts. Because different combinations of layer thicknesses and velocities can result in similar RF traces, it is necessary to create radial (or transverse) and vertical seismograms components using the algorithm of Randall, (1989). This algorithm is based on the reflection matrix of Kennett (1983) which provide consistent results for horizontal homogeneous layers. For the RF trace calculation, there are several available procedures, such as frequency-domain deconvolution (Langston, 1979), iterative time-domain deconvolution (Ligorria and Ammon, 1999), and autoregressive time-domain deconvolution (Wu et al. 2007). For seismograms associated with large earthquakes and high signal-to-noise ratios, all of these techniques have similar results. However, the time-domain methods are not affected by artificial effects introduced by equalization (Clayton and Wiggins, 1976). For this study, the method of Ligorria and Ammon, (1999) is used because of its inherent stability and minimal processing time.

3.2.1.2. – Surface wave dispersion

Relative to other forms of seismic energy, surface waves (e.g. Rayleigh and Love waves) have a low attenuation rate and broad frequency spectrum. These characteristics make surface-wave dispersion curves attractive for subsurface imaging over a range of shallow (Chourak et al., 2003; Jung et al., 2008) to deep structures (Van der Lee and Nolet, 1997; Mei et al., 2004). Given that the horizontal seismogram components are usually more affected by noise, dispersion curve processing for Love

waves is more difficult to achieve high fidelity resolution, especially for long period waveforms. For this reason, only the fundamental mode of Rayleigh wave group velocity dispersion curves are used in the joint inversion presented here. The equation for Rayleigh wave dispersion (Aki and Richards, 1980) is given by

$$U = \mathrm{d}\omega/\mathrm{d}k. \tag{2a}$$

In terms of the phase velocity c,

$$U = c + k\,\mathrm{d}c/\mathrm{d}k, \tag{2b}$$

where all variables are a function of the angular frequency ω, U is the group velocity, and k is the wave number.

The synthetic seismograms used to calculate Rayleigh wave dispersion curves are generated by algorithms described in Herrmann, (2002). Using the vertical component, the dispersion curves are calculated using the multi-filter technique (Dziewonski et al., 1969, Bhattacharya, 1983) which measures the signal amplitude variation as a function of velocity and frequency. Whereas the surface wave dispersion is primarily sensitive to the mean absolute value of seismic velocities, the receiver function is mainly sensitive to velocity contrasts. For this reason, the joint integration of both data sets can potentially reduce the non-uniqueness when modeling crustal features (Moreira et al., 2013).

3.2.1.3. – Magnetotelluric

MT sounding is a traditional geophysical method used to infer crust and mantle conductivities (Bologna et al. 2005, Gürer et al. 2004). The method requires simultaneous measurements of the natural magnetic fields and orthogonal electric fields. From these measurements, the electrical impedance can be found (Jones, 1992) by:

$$\begin{bmatrix} E_x \\ E_y \end{bmatrix} = \begin{bmatrix} Z_{xx} & Z_{xy} \\ Z_{yx} & Z_{yy} \end{bmatrix} \begin{bmatrix} H_x \\ H_y \end{bmatrix} \quad (3)$$

where E and H are the respective natural electric and magnetic fields recorded in orthogonal directions *x* and *y*, and Z_{ij} is the complex impedance tensor; and all variables are in the frequency domain. The apparent resistivity and phase can be calculated by:

$$\rho_{a,xy}(\omega) = (1/\omega\mu)|Z_{xy}(\omega)|^2 \quad (4)$$

and

$$\phi_{xy}(\omega) = \tan^{-1}[\text{Im } Z_{xy}(\omega)/\text{Re } Z_{xy}(\omega)] \quad (5)$$

where μ is the magnetic permeability, and ω is the angular frequency (previously defined). Similarly these equations can be applied to $\rho_{a,yx}(\omega)$ and $\phi_{yx}(\omega)$.

The synthetic data for transverse electric and transverse magnetic resistivity and phase are obtained using the finite-element solution for 2D models (Wannamaker et al.

1987), which presents higher stability for lower frequencies. Because the algorithm provides the resistivity and phase values, additional processing involving time-frequency transformation using cross-spectra are not necessary.

3.2.2. – Joint inversion

The joint inversion of disparate data sets is done by minimizing (in an iterative way) the least-squared differences between observed samples and the synthetic data in a multi-objective function. The algorithm used to update parameter values in the objective function is based on a linearized Gauss-Marquardt-Levenberg scheme, as described in Doherty (2005). In this algorithm the objective function is defined by:

$$\Phi = (\mathbf{c} - \mathbf{c}_0 - \mathbf{J}\,(\mathbf{b} - \mathbf{b}_0))^t\,\mathbf{Q}\,(\mathbf{c} - \mathbf{c}_0 - \mathbf{J}\,(\mathbf{b} - \mathbf{b}_0)) \qquad (6)$$

where the bold letters represent matrices (or vectors). In this equation, **c** represents the observed data vector, **b** is the parameters vector, **J** is the Jacobian matrix containing derivatives of each sample of vector **c** related to each parameter of vector **b** (which is responsible for the linearization of the proposed scheme), and **Q** is a diagonal matrix with the square weights of each observation. From this equation, it is possible to define an update parameter vector ($\mathbf{b}$-$\mathbf{b}_0$) as:

$$\mathbf{u} = (\mathbf{J}^t\,\mathbf{Q}\,\mathbf{J} + \alpha\,\mathbf{I})^{-1}\,\mathbf{J}^t\,\mathbf{Q}\,\mathbf{r} \qquad (7)$$

where **r** is the vector containing the observations residuals ($\mathbf{c}$-$\mathbf{c}_0$), **I** is the identity matrix and α is the Marquardt parameter (introduced to stabilize the update parameter process).

The vector **u** therefore forms the basis for non-linear parameter estimation through weighted least squares approach. For crustal and upper mantle lithologies shear wave velocities can vary from 3 to 5.5 km/s (Christensen and Mooney, 1995) while electric resitivity varies from 10^{-2} to 10^{6} Ωm (Korja, 1997), therefore the Jacobian matrix elements can have different magnitudes and mislead the update vector calculation. For this reason, a scaling matrix is introduced in the previous equation:

$$\mathbf{S}^{-1}\,\mathbf{u} = ((\mathbf{J}\,\mathbf{S})^{t}\,\mathbf{Q}\,\mathbf{J}\,\mathbf{S} + \alpha\,\mathbf{S}^{t}\,\mathbf{S})^{-1}\,(\mathbf{J}\,\mathbf{S})^{t}\,\mathbf{Q}\,\mathbf{r} \qquad (8)$$

where $S_{ii} = (\mathbf{J}^{t}\mathbf{Q}\mathbf{J})_{ii}^{-1/2}$, keeping the equation (6) mathematically equivalent to equation (5).

The algorithm is versatile and can be applied to any geophysical data and parameters. In this study, the previously described seismic and MT methods are used in the forward model calculations, and the Gauss-Marquardt-Levenberg method is used to estimate the model parameters.

3.2.3. – Cross-gradient constraint

Because this inversion uses parameters with different physical properties, the inclusion of different data sets to the same objective function may not increase model resolution, improve precision of the estimated models, or enhance convergence and stability. For this reason, the cross-gradient constraint (Gallardo and Meju, 2004) is added to the joint inverse procedure. This constraint implies that there is structural similarity between the resistivity and velocity models, resulting in the co-location of

contrasts among the parameter sets. The cross-gradient constraint is applied as a new observation group following the cross-product:

$$g(x,y,z) = \nabla r(x,y,z) \times \nabla s(x,y,z) = 0, \quad (9)$$

where *r* and *s* represents the respective resistivity and velocity parameters, and *x*, *y* and *z* are the three dimension coordinates. This equation does not represent discontinuities or singularities; therefore, it can be readily incorporated into the linearized inversion scheme. In considering a 2D model, the discrete cell grid (figure 1) can be rewritten as:

$$g \approx (4/\Delta x \Delta z)\,[r_{ij}(s_{(i+1)j} - s_{i(j+1)}) + r_{i(j+1)}(s_{ij} - s_{(i+1)j}) + r_{(i+1)j}(s_{i(j+1)} - s_{ij})] = 0, \quad (9.1)$$

or

$$g \approx (4/\Delta x \Delta z)\,[s_{ij}(r_{i(j+1)} - r_{(i+1)j}) + s_{i(j+1)}(r_{(i+1)j} - r_{ij}) + s_{(i+1)j}(r_{ij} - r_{i(j+1)})] = 0 \quad , \quad (9.2)$$

where the subscript letter *i* represents the cell row (z direction) and *j* represents the cell column (x direction). If both models have co-located anomalies then both vectors in the right-hand-side of equation (7) will be of the same (or opposite) sign (regardless of the vectors length) and the vector g will be zero. One possible solution in both equations (9.1) and (9.2) is that the difference between two adjacent cells of the same model should be zero, meaning that the cross-gradient constraint reflects a smooth (homogeneous) constraint.

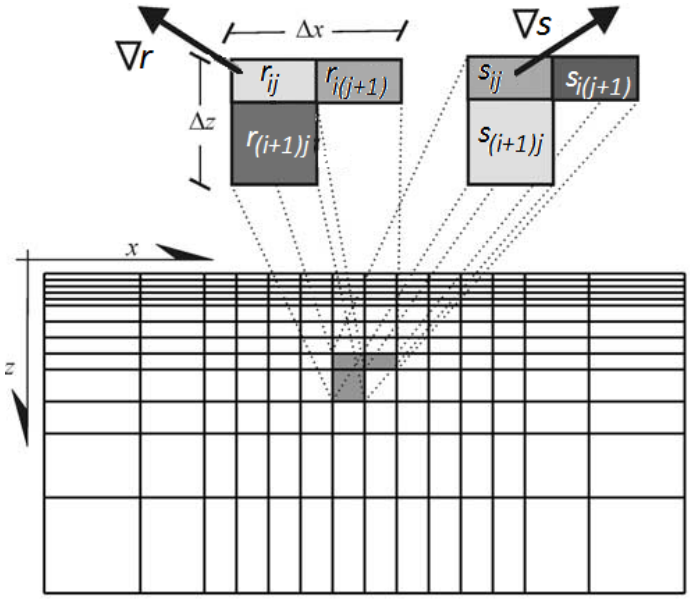

Figure 3.1. Discrete representation of cross-gradient constraint for a 2D grid. Adapted from Gallardo and Meju, 2004.

3.3. – Synthetic test

The proposed methodology was tested with synthetic data obtained using the physical model represented in figure 3.2. The main geological features being modeled as geophysical soundings include a sedimentary basin, an upper and lower crust, and an upper mantle. This geological model characterizes crustal features such as the Conrad (between upper and lower crust) and Moho (between lower crust and upper mantle) discontinuities. The numerical model reflects a 2D grid with 3 homogeneous layers over half-space with sharp contrasts between each layer co-located in both resistivity and velocity parameter groups. The profile reflects typical MT soundings (Korja, 1997) and deep enough to represent the Moho discontinuity and the upper mantle. This profile was divided into 3 different regions each of which incorporated one seismic station, showing a lateral variation in layers depth and a low velocity zone (LVZ) with low resistivity values on the left portion.

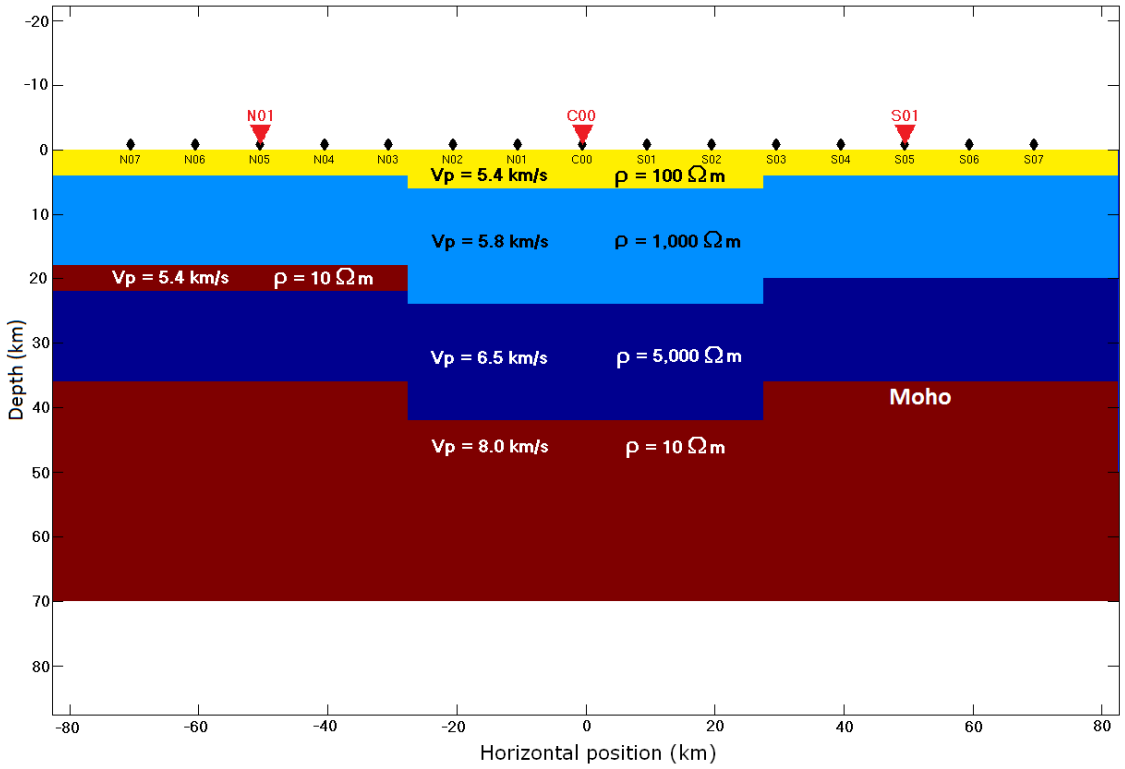

Figure 3.2. Homogeneous synthetic model of resistivity and velocity parameters with lateral variation of layers depth and a low velocity-resistivity zone on the left portion.

In figure 3.2 the black dots represent MT stations, and the inverted red triangles are seismic stations. The apparent resistivity and phase curves for transverse electric and transverse magnetic data were generated for each station using the algorithm of Wannamaker et al. (1987). Random noise characterized as a Gaussian distribution was added (3% for resistivities and 2.5° for phase, slightly higher than Agarwal et al. 1993 and Pek and Santos, 2006) to each curve. The 1D model profiles underlying seismic stations were used to generate synthetic seismograms. The seismograms used in the RF calculation were contaminated by Gaussian random noise with 2% of the direct P wave amplitude and the seismograms for surface dispersion curves calculation were also contaminated by 2% Gaussian random noise.

The P-to-S converted phase at the Moho discontinuity and multiples reflections

within the crust usually occur on the first 30 seconds of the seismogram and after the first P arrival. To ensure that all crustal features were well represented in each RF trace, synthetic seismograms were generated with a 60 second length. These seismograms were then deconvolved using the algorithm of Ligorria e Ammon (1999) with up to 500 iterations. The synthetic seismograms used for dispersion curve calculations were generated using software provided by Herrmann (2002). In turn, the dispersion curves were then calculated using the multi-filter technique (Dziewonski et al. 1969, Bhattacharya, 1983).

Initially separate inversions were carried out for each of the parameter groups and then the joint inversion of all data set with the cross-gradient constraint. Due to the high number of parameters and consequently high degree of non-linearity, the linearized method for joint inversion becomes more sensitive to the initial parameter values often times converging to local minima and non-realistic models. To avoid this issue, the estimated parameters for separate inversions were used as initial values for the same parameters in the joint inversion. This process promoted convergence to solutions based on global minima.

3.3.1. – Separate inversions

The synthetic model has three seismic stations resulting in three 1D subsurface profiles. Given that receiver function and surface wave dispersion map seismic velocity, both data sets were jointly inverted to estimate a common set of seismic velocity parameters. For this inversion, a smooth constraint was added to adjacent parameters in the same profile (vertical smoothness) and parameters at same depth in adjacent profiles (horizontal smoothness). The results for each profile are shown in figure 3.3. Inspection

of this figure provides a visual comparison of the estimated and known parameters. Besides differences among original and estimated values for the three profiles, the velocity models correctly represent the main crustal discontinuities, including the low velocity zone (LVZ) on the N01 profile, where the higher differences happening in the layers of upper mantle, below Moho. The receiver function traces obtained from the original and estimated models are presented in figure 3.4. The main peaks representing the seismic waves refraction through the main crustal discontinuities are present (Conrad P-to-S conversion around 3 seconds and Moho P-to-S conversion around 5 seconds), however with relative difference among RF samples about 30% for the Moho P-to-S conversion peak of station N01, about 5% for station C00 and about 20% for station S01. The dispersion curves for both models depict excellent correspondence between the original and estimated values with absolute of residuals less than 10^{-2} km/s (0.3%) for all SWD samples of the three stations (figure 3.5).

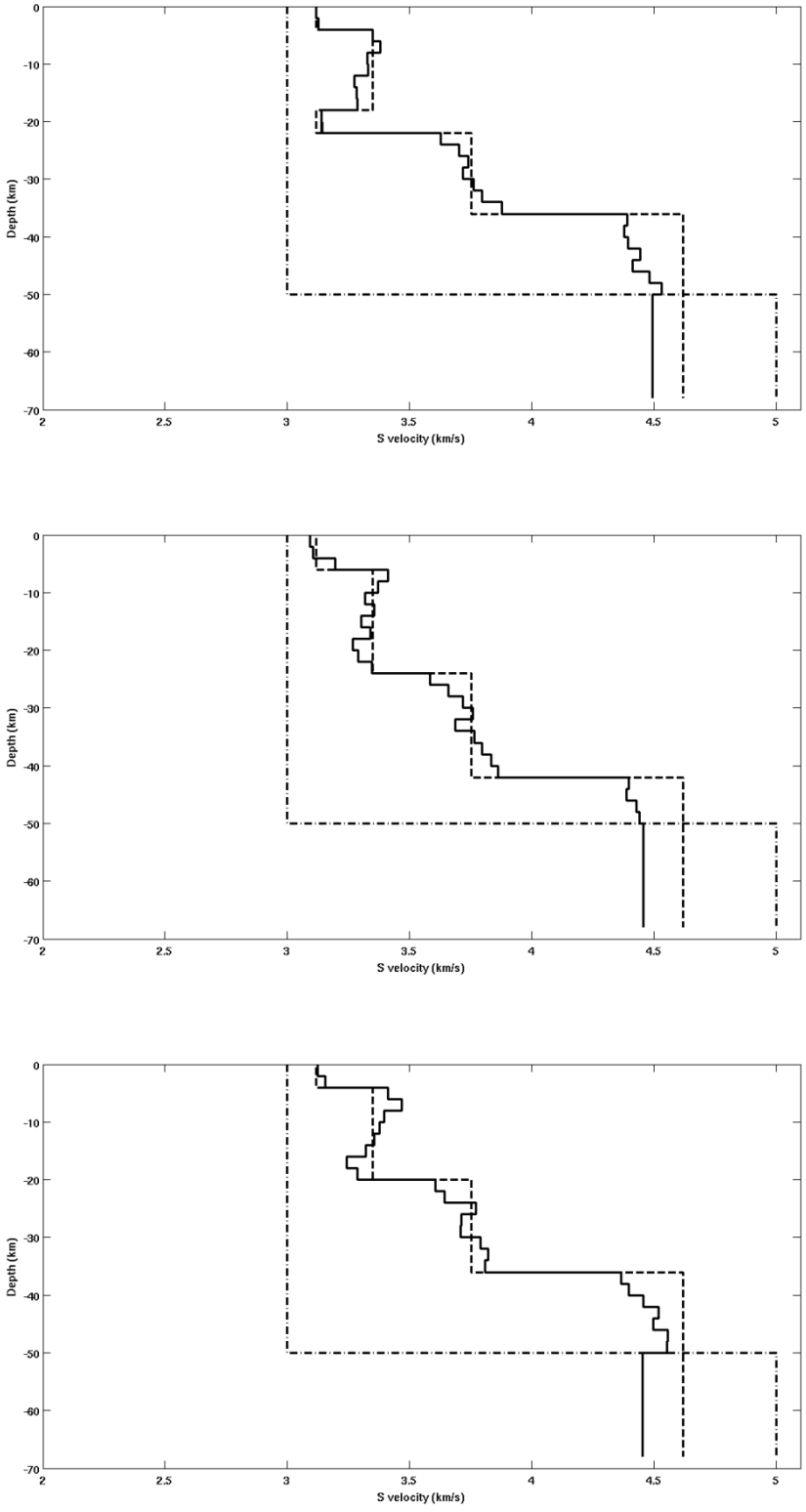

Figure 3.3. Calibration results for profiles N01 (top), C00 (center) and S01 (bottom), comparing the initial (dash-point), original (dashed) and estimated (solid) parameters values.

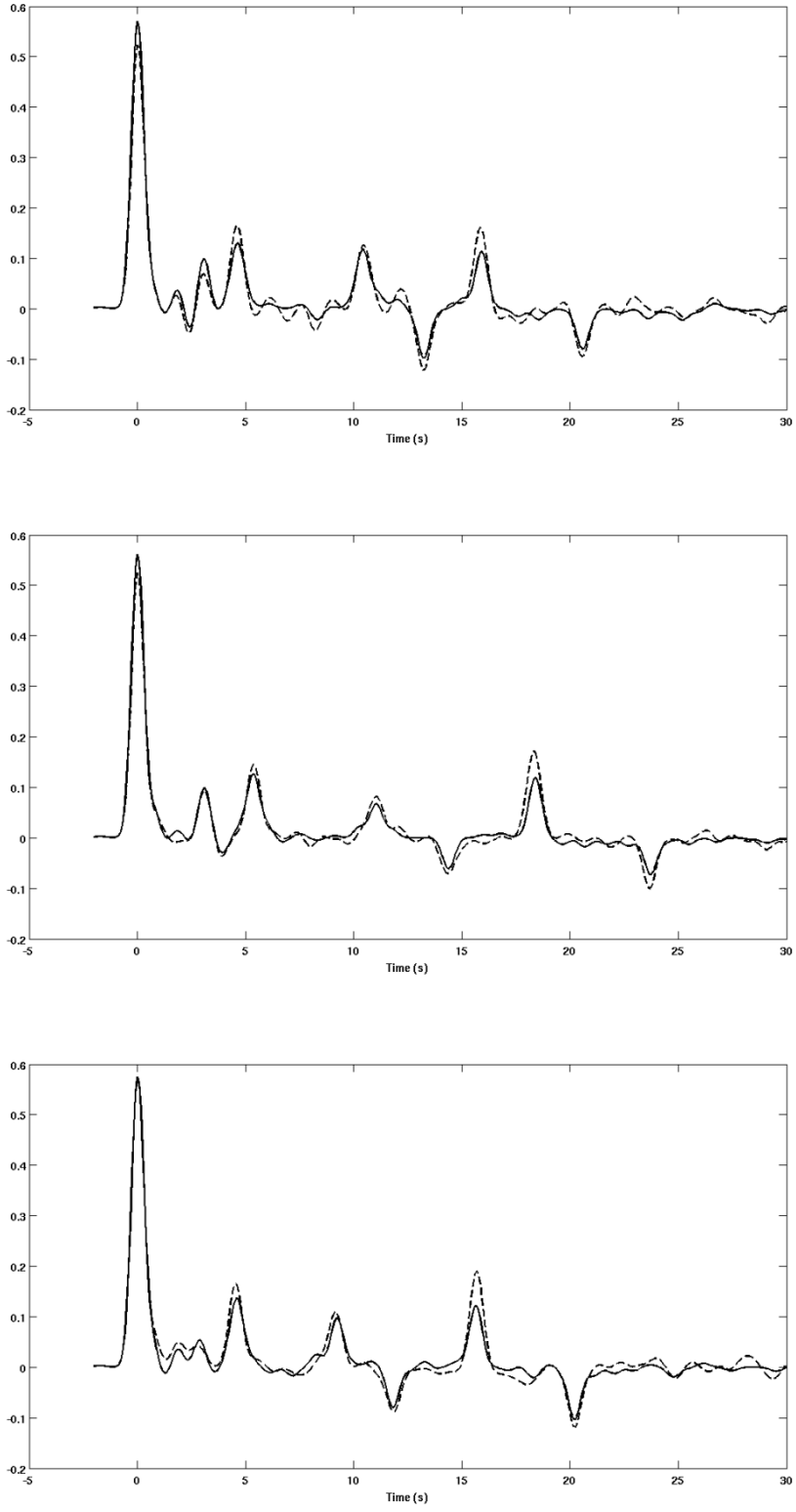

Figure 3.4. Receiver function traces from original (dashed) and estimated (solid) models for the profiles N01 (top), C00 (center) and S01 (bottom)

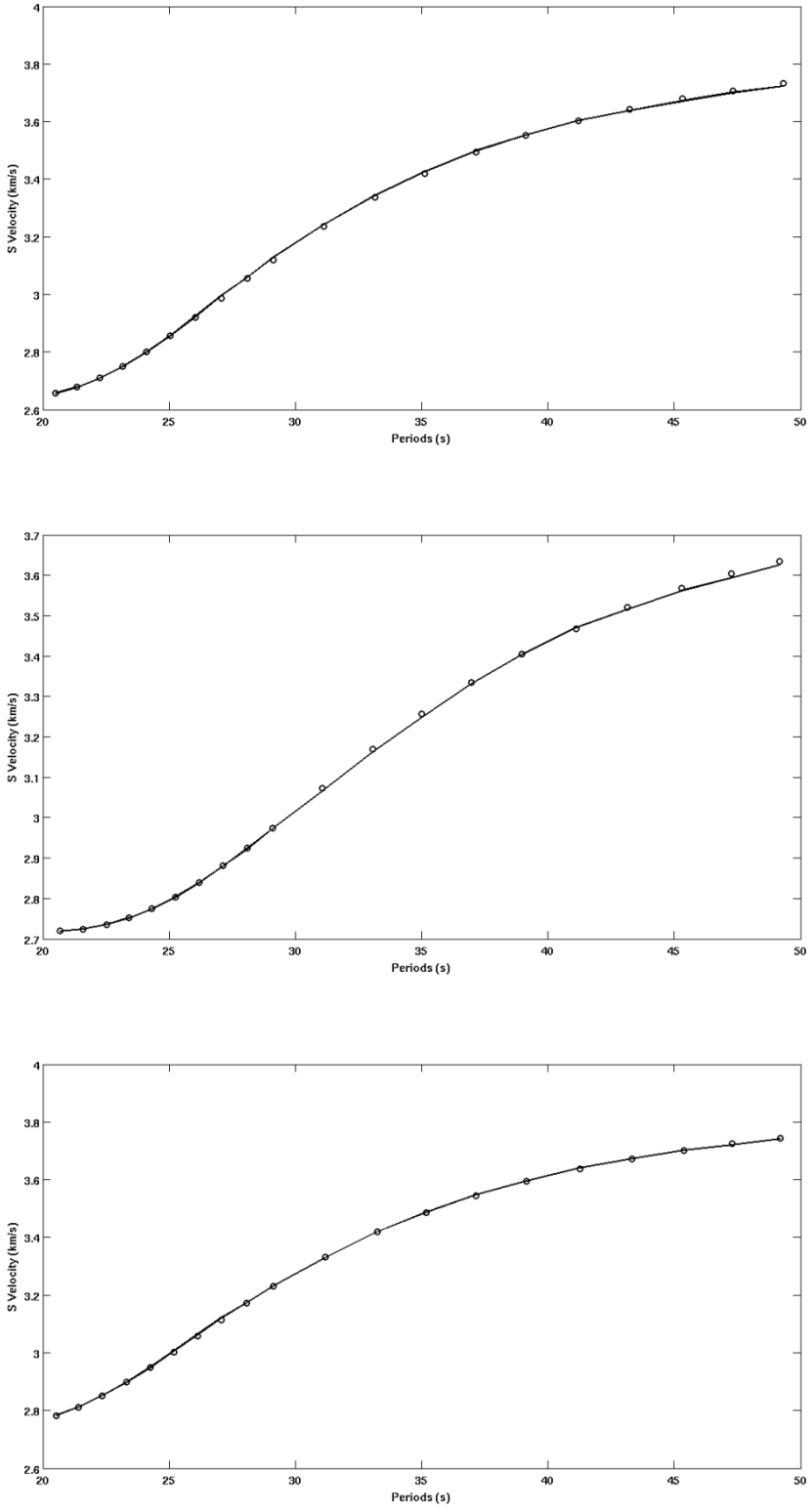

Figure 3.5. Dispersion curves from synthetic (circle) and estimated (red solid line) models for the profiles N01 (top), C00 (center) and S01 (bottom)

The 2D resistivity model is resolved using 15 MT stations equally separated along a 150 km length profile. As with the seismic velocity inversion, a smooth constraint was added between adjacent cells in both horizontal and vertical directions. The results presented in figure 3.6 reveal poor resolution when using the traditional MT inversion to image lateral variations as well as a loss of vertical resolution with depth. The apparent resistivity and phase for three stations (MT stations co-located with seismic stations) are shown in figure 3.7. The differences between each curve are minimal with absolute residuals less than 10^{-1} Ωm (0.2%) for all MT apparent resistivity samples and less than 2º (4.5%) for all phase samples.

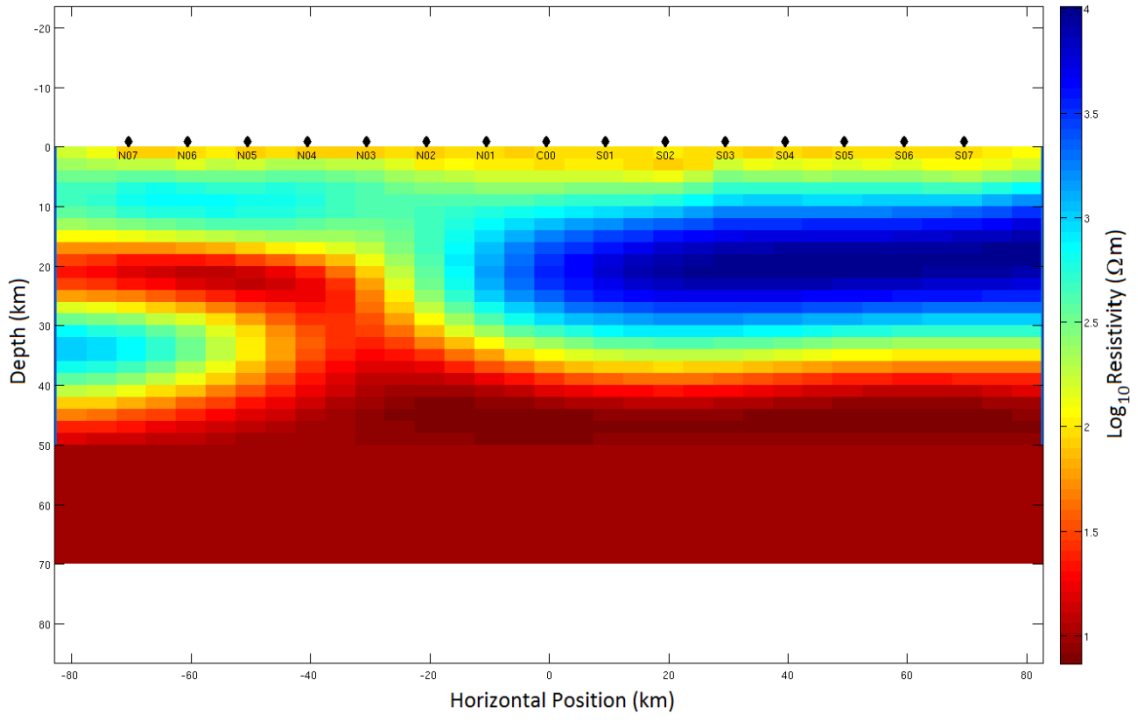

Figure 3.6. Estimated resistivity parameters for MT inversion. The vertical resolution is limited and the true model lateral variation is not imaged.

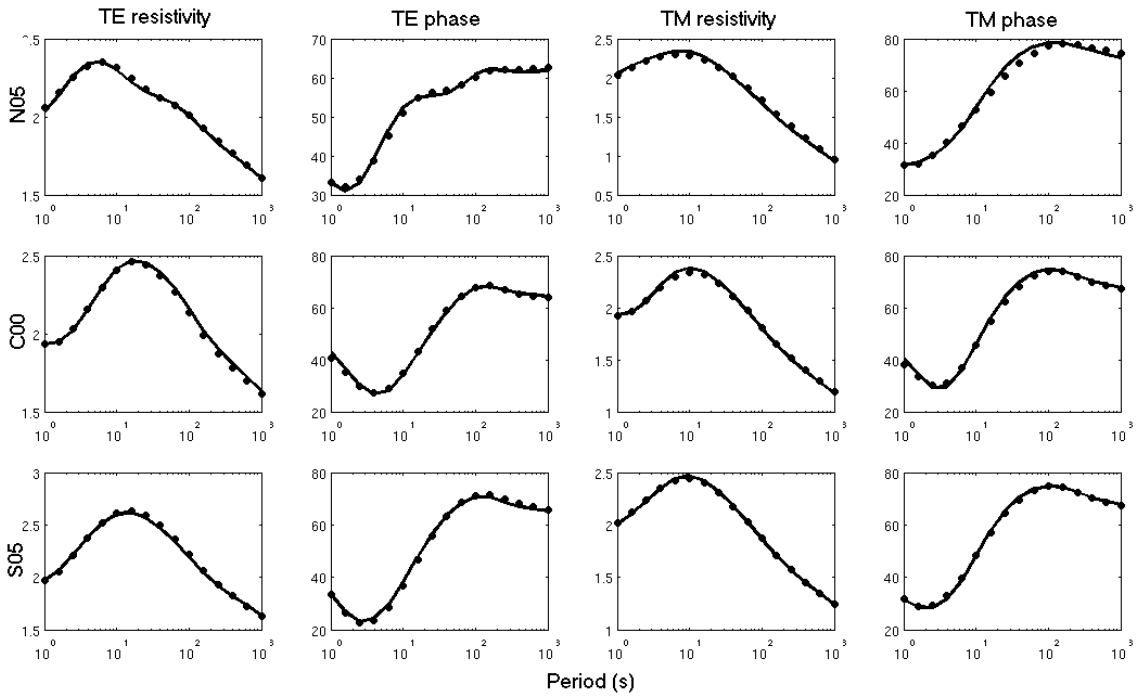

Figure 3.7. Apparent resistivity and phase for three MT stations with synthetic (dots) and estimated (solid line) samples.

3.3.2. – Joint inversion

Using the proposed scheme, the resistivity and velocity parameters were jointly inverted. The seismic station N01 is co-located with MT station N05, the same way seismic stations C00 and S01 are co-located with MT stations C00 and S05 respectively. To make possible the application of the cross-gradient equation (9), the seismic velocity parameters were duplicated from each 1D profile in the proximities of respective seismic stations, creating a quasi-2D profile grid. Because the cross-gradient equation includes a smooth constraint, this additional information was not added to the inversion. The estimated results for the three seismic 1D profiles and 2D resistivity profile are shown in figures 3.8 and 3.9, respectively.

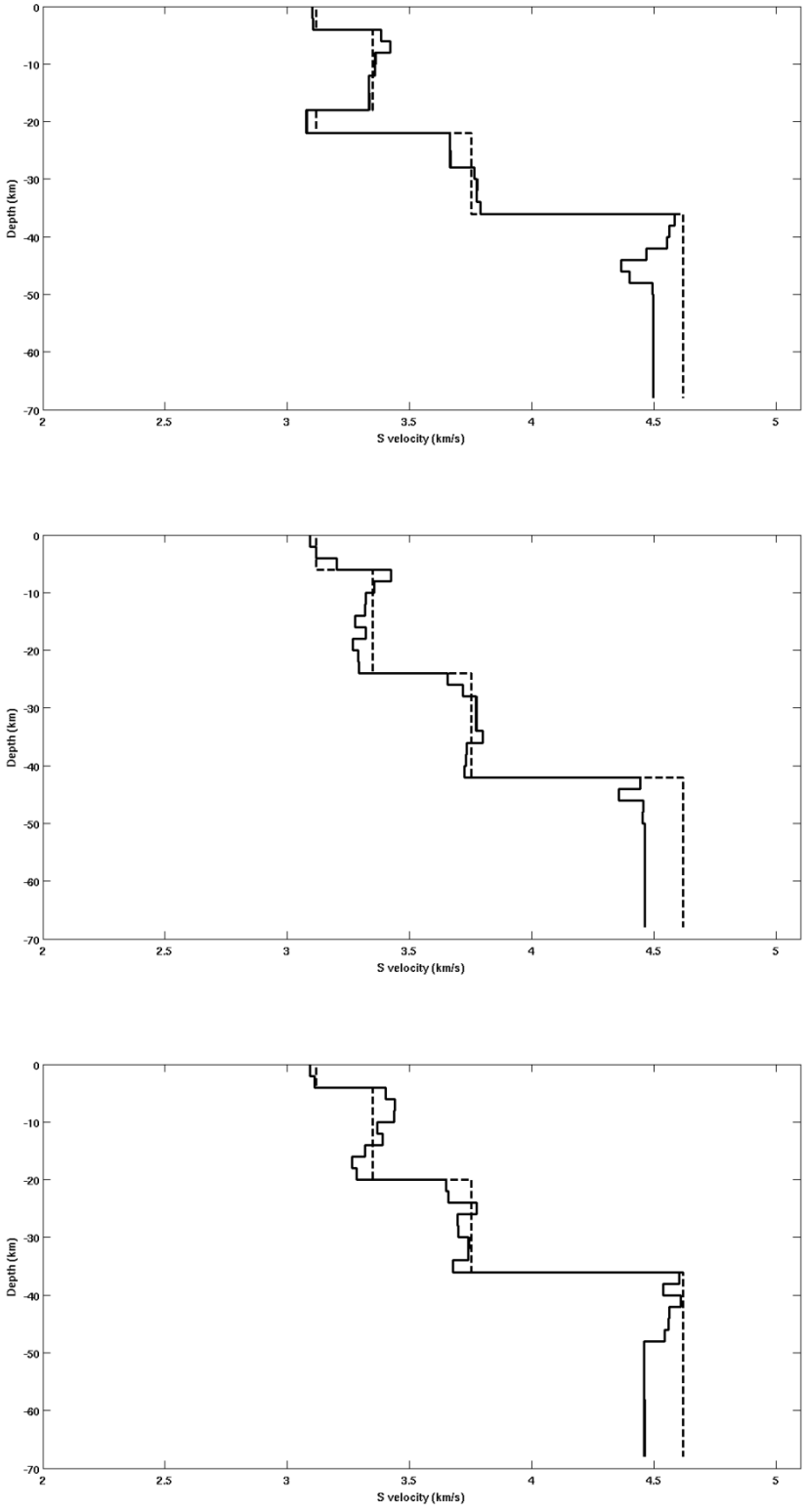

Figure 3.8. Joint inversion results for N01 (top), C00 (center) and S01 (bottom) seismic profiles with synthetic (dashed) and estimated (solid) parameters values.

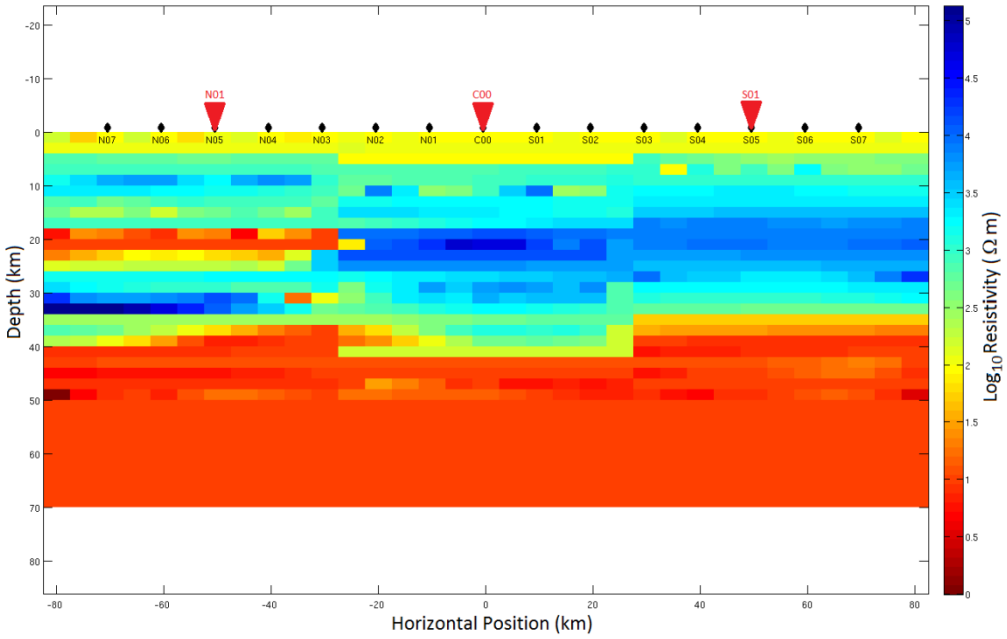

Figure 3.9. Joint inversion results for resistivity parameters.

In comparing the 1D seismic profile results for separate and joint inversions reveals visual improvement in the absolute values of parameters close to the main discontinuities, especially the layers below Moho, where the difference among estimated and synthetic parameters reduced from 5% to 1.1% for station N01, from 4.6% to 4.2% for station C00 and from 4.6% to 0.7% for station S01. For the resistivity model, the improvement is more noticeable comparing the results from separate and joint inversions with the synthetic model where the average difference between the estimated and synthetic parameters reduced from 0.678 Ωm to 0.436 Ωm (reduction of 35%) for the entire profile and from 1.829 Ωm to 0.985 Ωm (reduction of 46%) considering only the left portion underlying the low resistivity zone. These improvements make it possible to see the discontinuities between the sediment basin and upper crust, and between the lower crust and upper mantle (Moho). This is especially obvious on the left portion of the figure, where the higher resistivity layer below the low velocity-resistivity zone is now properly imaged.

3.4. – Conclusions

The joint inversion of receiver function, surface wave dispersion and magnetotelluric data provides improved imaging capability over the traditional inversion of independent data sets. Integrating the three data sets using the proposed multi-component objective function and cross-gradient constraint provides simultaneous reconstructions with improved 2D resistivity and 1D seismic velocity models for identifying lateral variations and vertical resolution of crustal features. The feasibility of MT soundings co-located to broadband seismic stations or installation of seismic stations in previously sounded MT profiles makes the proposed methodology useful for crustal tectonic and geologic studies or subsurface mineral deposit assessment. The comparative improvements in estimated models support the use of joint-geophysical application in future crustal studies.

3.5. – Computational resources

Computer software package for seismic forward model is encapsulated in Computer Programs in Seismology provided by C. Ammon and R. Herrmann upon request at http://www.eas.slu.edu/eqc/eqccps.html (last accessed January 2013). Magnetotelluric forward model calculation is encapsulated in Occam2DMT software provided by the Marine EM Laboratory of the Scripps Institution of Oceanography (http://marineemlab.ucsd.edu/Projects/Occam/2DMT/index.html, last accessed January 2013). Inversion algorithm is encapsulated in Parameter Estimation (PEST) package provided by John Doherty at www.pesthomepage.org (last accessed June 2012). Some figures were created using Matrix Laboratory (MATLAB, www.mathworks.com, last

accessed June 2011).

3.6. – Acknowledgements

LM was fully supported by CAPES and CAPES/Fulbright 23038.034805/2009-71 grants. GSF is supported by CNPq PQ grants.

3.7. – References

Agarwal, A.K., Poll, H.E., and Weaver, J.T. 1993. One- and two- dimensional inversion of magnetotelluric data in continental regions. Phys. Earth Planet. Inter. 81, 155-176.

Aki, K., Richards, P.G. 1980. Quantitative Seismology: Theory and Methods, Vol. 1 and 2, W. H. Freeman, San Francisco.

Ammon, C.J., 1991. The isolation of receiver effects from teleseismic P waveforms. Bull. Seismol. Soc. Amer., 81(6), 2504-2510.

An, M., Assumpção, M.S., 2004. Multi-objective inversion of surface wave and receiver functions by competent genetic algorithm applied to the crustal structure of the Parana Basin, SE Brazil, Geophys. Res. Lett. **31**, L05615, doi:10.1029/2003GL019179.

Bhattacharya, S.N., 1983. Higher order accuracy in multiple filter technique. Bull. Seism. Soc. Am. 73, 1395-1406.

Bedrosian, P.A., Maercklin, N., Weckmann, U., Bartov, Y., Ryberg, T., Ritter, O., 2007. Lithology-derived structure classification from the joint interpretation of magnetotelluric and seismic models, Geophys. J. Int. 170, 737–748.

Bodin, T., Sambridge, M., Tkalčić, H., Arroucau, P., Gallagher, K., Rawlinson, N., 2012. Transdimensional inversion of receiver functions and surface wave dispersion. J. Geophys. Res. 117, B02301. doi:10.1029/2011JB008560

Bologna, M.S., Padilha, A.L., Vitorello, I., 2005. Geoelectric crustal structures off the SW border of the São Francisco craton, central Brazil, as inferred from a magnetotelluric survey . Geophys. J. Int. 162, 357-370.

Chourak, M., Corchete, V., Badal, J., Serón, F., Gómez, F., 2003. Imaging of the near-surface shear-wave velocity structure of the Granada Basin (Southern Spain). Bull. Seismol. Soc. Amer. 93(1), 430-442.

Clayton, R.W., and Wiggins, R.A., 1976. Source shape estimation and deconvolution of teleseismic body waves, J. R. Astr. Soc. **47**, 151- 177.

Christensen, N. I., and Mooney, W. D., 1995. Seismic velocity structure and composition the continental of crust: A global view. J. Geophys. Res., vol. 100, B7, 9761-9788.

Doherty, J., 2005. PEST: Model-Independent Parameter Estimation. User manual, 5th edition. Watermark Numerical Computing, Brisbane, Australia, pp. 336.

Dziewonski, A., Bloch, S., Landisman, M., 1969. A technique for the analysis of transient seismic signals. Bull. Seismol. Soc. Amer. 59(1), 427-444.

Gallardo, L.A., Meju, M.A., 2004. Joint two-dimensional DC resistivity and seismic travel time inversion with cross-gradients constraints. J. Geophys. Res. 109, B03311, doi:10.1029/2003JB002716.

Gallardo, L.A., Meju, M.A., 2007. Joint two-dimensional cross-gradient imaging of magnetotelluric and seismic traveltime data for structural and lithological classification. Geophys. J. Int. 169, 1261–1272.

Gürer, A., Bayrak, M., Gürer, Ö.F., 2004. Magnetotelluric images of the crust and mantle in the southwestern Taurides, Turkey. Tectonophysics 391, 109 – 120.

Herrmann, R.B., 2002. Computer Programs in Seismology - An overview of synthetic seismogram computation. St. Louis University, St. Louis, MO.
URL http://www.eas.slu.edu/People/RBHerrmann/ComputerPrograms.html.

Jones, A.G., 1992. Electrical conductivity of the continental lower crust. In: Fountain, D.M., Arculus, R.J., Kay, R.W. (Eds.), The Lower Continental Crust, pp. 81- 143. Elsevier, Amsterdam.

Jung, H., Jang, Y., Lee, J.M., Moon, W.M., Baag, C.E., Kim, K.Y., Jo, B.G., 2008. Shallow-depth shear wave velocity structure of the Southern Korean Peninsula obtained

from two crustal-scale refraction profiles. Journal of Applied Geophysics 66, 59-69.

Kennett, B.L.N., 1983. Seismic Wave Propagation in Stratified Media, Cambridge University Press, Cambridge, England, 342 pages.

Korja, T., 1997. Electrical Conductivity of the Lithosphere - Implications for the Evolution of the Fennoscandian Shield . Geophysica, 33(1), 17-50.

Langston, C.A., 1979. Structure under Mount Rainier, Washington, inferred from teleseismic body waves, J. Geophys. Res. 84, 4749–4762.

Ligorria, J.P., Ammon, C.J., 1999. Iterative deconvolution and receiver-function estimation, Bull. Seismol. Soc. Am. 89(5), 1395–1400.

Mei, F., Assumpção, M., Van der Lee, S., 2004. Group-velocity tomography and lithospheric S-velocity structure of the South American continent. Phys. Earth Planet. Inter. 147, 315-331.

Meju, M.A., Gallardo, L.A., Mohamed, A.K., 2003. Evidence for correlation of electrical resistivity and seismic velocity in heterogeneous near-surface materials, Geophys. Res. Lett. 30(7), 1373-1376, doi:10.1029/2002GL016048.

Moreira, L.P., Friedel, M.J., França, G.S., 2013. Uncertainty analysis in the joint inversion of receiver function and surface-wave dispersion, Paraná Basin, southeast Brazil. Bull. Seism. Soc. Am. 103(3).

Moorkamp, M., Jones, A.G., Eaton, D.W., 2007. Joint inversion of teleseismic receiver functions and magnetotelluric data using a genetic algorithm: Are seismic velocities and electrical conductivities compatible? Geophys. Res. Lett. 30, L16311, doi:10.1029/2007GL030519.

Moorkamp, M., Jones, A.G., Fishwick, S., 2010. Joint inversion of receiver functions, surface wave dispersion, and magnetotelluric data. J. Geophys. Res. 115, B04318, doi:10.1029/2009JB006369.

Pasyanos, M.E., Walter, W.R., Hazler, S.E., 2001. A surface wave dispersion study of the Middle East and North Africa for monitoring the Comprehensive Nuclear-Test-Ban Treaty. Pure Appl. Geophys. 158, 1445–1474

Pek, J., and Santos, F.A.M. 2006. Magnetotelluric inversion for anisotropic conductivities in layered media. Phys. Earth Planet. Inter. 158, 139-158.

Randall, G.E., 1989. Efficient calculation of differential seismograms for lithospheric receiver functions, Geophys. J. Int. 99, 469–481.

Ritzwoller, M.H., Levshin, A.L., 1998. Eurasian surface wave tomography: group velocities. J. Geophys. Res. 103 (B3), 4839–4878.

Van der Lee, S., Nolet, G., 1997. Uppermantle Svelocity structure of North America. J. Geophys. Res. 102 (B10), 22815–22838.

Wannamaker, P.E., Stodt, J.A., Rijo, L., 1987. A stable finite-element solution for two-dimensional magnetotelluric modeling, Geophysical Journal of the Royal Astronomical Society 88, 277–296.

Wu, Q, Li, Y., Zhang, R., Zeng, R., 2007. Receiver Functions from Autoregressive Deconvolution. Pure appl. Geophys. 164, 2175–2192.

Zevallos, I., Assumpcao, M., Padilha, A.I., 2009. Inversion of teleseismic receiver function and magnetotelluric sounding to determine basement depth in the Paraná Basin, SE Brazil. Journal of Applied Geophysics 68, 231–242.

4. – Conclusões

A análise de incertezas de inversão conjunta de dados de função do receptor e dispersão de ondas de superfície representa um importante papel na modelagem crustal de velocidade de ondas sísmicas, pois define uma faixa de valores para os parâmetros de velocidade de ondas sísmicas para um intervalo de confiança pré-determinado. Os métodos utilizados até o presente possuem grandes simplificações ou são de natureza qualitativa, sem formalidades matemáticas. Assim, a metodologia proposta para determinação das incertezas baseadas na predição de valores observados representa uma importante contribuição para essa área da geofísica. Os testes realizados, bem como sua utilização em dados coletados na bacia do Paraná, mostraram a aplicação do método e seus resultados, consistindo em um conjunto de modelos 1D, cada um deles representando um ponto crítico na região de mínimo da função objetivo, formando um conjunto de valores em torno do valor estimado no processo de inversão, gerando informação tanto da distribuição estatística dos modelos dentro do intervalo de confiança bem como os limites desse intervalo e seus respectivos percentis.

A incorporação de múltiplos dados geofísicos dentro de um único processo de inversão, configurando uma inversão conjunta, tem como resultado esperado uma redução da não-unicidade e maior robustez do processo com relação a ruídos nos dados observados. Essa incorporação, entretanto, requer informações adicionais para estabilização do algoritmo numérico, tais como relações matemáticas entre os parâmetros invertidos e vínculos e informação a priori. A inversão conjunta de dados de função do receptor, dispersão de ondas superficiais e magnetotelúricos tem como proposta aumentar a resolução dos resultados e minimizar os efeitos das limitações que cada um dos métodos apresenta separadamente, como por exemplo a baixa resolução

lateral da inversão utilizando dados magnetotelúricos. A metodologia proposta de inversão conjunta desses dois grupos de parâmetros geofísicos, com o vínculo estrutural do gradiente cruzado, se mostrou eficiente na resolução das principais feições geológicas simuladas no modelo sintético, aproximando o modelo estimado bem próximo do modelo real. Além disso o aprimoramento da inversão conjunta em comparação com a inversão de cada grupo de dados separadamente é notório e evidente, validando o método proposto.

A partir dos resultados obtidos e pela relevância desses resultados, a presente tese é considerada por seus autores como importante contribuição científica para a comunidade geofísica.